Theory of the orthogonal dimer Heisenberg spin model for $SrCu_2(BO_3)_2$

2003 J. Phys.: Condens. Matter 15 R327

(http://iopscience.iop.org/0953-8984/15/9/201)

INSTITUTE OF PHYSICS PUBLISHING JOURNAL OF PHYSICS: CONDENSED MATTER

J. Phys.: Condens. Matter **15** (2003) R327–R366 PII: S0953-8984(03)31442-0

TOPICAL REVIEW

Theory of the orthogonal dimer Heisenberg spin model for $SrCu_2(BO_3)_2$

Shin Miyahara[1,2] **and Kazuo Ueda**[2]

[1] Institut de Physique Théorique, BSP, Université de Lausanne, CH-1015, Switzerland
[2] Institute for Solid State Physics, University of Tokyo, Kashiwanoha, Kashiwa-shi, Chiba 277-8581, Japan

E-mail: Shin.Miyahara@ipt.unil.ch

Received 6 January 2003
Published 24 February 2003
Online at stacks.iop.org/JPhysCM/15/R327

Abstract

The magnetic properties of $SrCu_2(BO_3)_2$ are reviewed from a theoretical point of view. $SrCu_2(BO_3)_2$ is a new two-dimensional spin gap system and its magnetic properties are well described by a spin-1/2 antiferromagnetic Heisenberg model of the orthogonal dimer lattice. The model has a dimer singlet ground state whose exactness was proven by Shastry and Sutherland for a topologically equivalent model more than 20 years ago. The exactness of the ground state is maintained even if interlayer couplings are introduced for $SrCu_2(BO_3)_2$. In the two-dimensional model, quantum phase transitions take place between different ground states for which three phases are expected: a gapped dimer singlet state, a plaquette resonating valence bond state and a gapless magnetic ordered state. Analysis of the experimental data shows that the dimer singlet ground state is realized in $SrCu_2(BO_3)_2$. The orthogonality of the dimer bonds, which is the underlying symmetry of the exactness of the ground state, also leads to an unusual property of elementary excitations, namely the almost localized nature of the triplet excitations. Application of an external magnetic field changes the density of the triplet excitations. In general, there is competition between kinetic energies and interaction energies between triplets. The almost localized nature of the triplets makes it easy to form regular lattices. In fact, at certain densities, where the commensurability energy is significant, the triplet excitations form superstructures and plateaux appear at 1/2, 1/3, 1/4 and 1/8 in the magnetization curve. In high-magnetic-field experiments, magnetic plateaux at magnetizations of 1/3, 1/4 and 1/8 have been observed. Translational symmetry of the lattice is spontaneously broken at the plateaux, except for the 1/2 plateau. The 1/3 and 1/4 plateaux are expected to have magnetic superstructures of stripe form while the 1/2 plateau has a square unit cell and the 1/8 plateau a rhomboid cell. Especially at the 1/8 plateau, nuclear magnetic resonance experiments indicate the presence of at least 11 distinct Cu sites with different spin polarizations, which is the first evidence of breaking of the translational symmetry at the plateau phase. The spin texture calculated

on the basis of a Heisenberg model with adiabatic spin–phonon coupling is consistent with the experimental results.

Contents

1. Introduction

Low-dimensional quantum spin systems are one of the hot topics in present-day condensed matter physics, both experimentally and theoretically [1–3]. In such a system the effects of quantum fluctuations are important; owing to them, particularly in systems with geometrical frustration, a gapped spin-singlet ground state may appear. In general there is competition between such a nonmagnetic ground state and a magnetically ordered state, which is expected from classical theories. The order–disorder transition, which may be tuned by changing some parameter of quantum spin systems, is one of the simplest possible examples of a quantum phase transition phenomenon.

As a well-known example of a quantum phase transition, let us consider the spin-1/2 zig-zag chain Heisenberg model, which is shown in figure 1 [4]. It has been shown that for $J_2/J_1 > 0.2411$ the ground state is nonmagnetic and has a spin gap [5]. On the other hand, the model has quasi long-range order for $J_2/J_1 < 0.2411$. Therefore a quantum phase transition takes place from the gapped state to the gapless state at $J_2/J_1 = 0.2411$ with increase in the parameter J_2/J_1.

It should be emphasized that at $J_2/J_1 = 0.5$, the nonmagnetic ground state is known exactly:

$$\Psi = \prod_a \frac{1}{\sqrt{2}}(|\uparrow\downarrow\rangle_a - |\downarrow\uparrow\rangle_a). \tag{1}$$

Here a denotes one type of nearest-neighbour bonds, for example A-dimers (see figure 1). The model with $J_2/J_1 = 0.5$ is called the Majumdar–Ghosh model after the people who discovered the exact ground state of equation (1) [4].

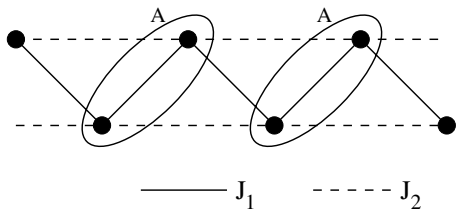

Figure 1. Zig-zag chain model. This consists of two types of bond: nearest-neighbour bonds J_1 and next-nearest-neighbour bonds J_2. Let us define the J_1 bonds marked by ellipses as A bonds and the other J_1 bonds as B bonds. The product of the singlet states on A bonds or B bonds is the exact ground state for $J_2/J_1 = 0.5$.

Because of these nontrivial quantum phenomena, low-dimensional quantum spin models whose ground states have a spin gap, like the zig-zag chain model, have been studied extensively from both experimental and theoretical points of view. In particular, many investigations on two-dimensional systems with spin gaps have been carried out, stimulated by the pseudo spin gap behaviours observed in high T_c cuprates. As by-products of this type of investigation, several new spin gap systems have been found. Some of the examples include the coupled spin ladder systems, $SrCu_2O_3$ [6], CaV_2O_5 [7] and the plaquette resonating-valence-bond system, CaV_4O_9 [8].

Another example of nontrivial quantum phenomena in low-dimensional spin systems is the presence of intermediate plateaux in the magnetization curve. The investigation of magnetization plateaux started theoretically for one-dimensional spin systems, for example a spin-1/2 ferromagnetic–ferromagnetic–antiferromagnetic Heisenberg chain [9, 10] and spin-1 antiferromagnetic Heisenberg chain with bond alternation [11, 12]. A necessary condition for the existence of plateaux in one-dimensional systems was obtained by Oshikawa *et al* [13]. They conclude that the occurrence of a magnetization plateau is possible when the following condition is satisfied:

$$n(S - m) = \text{integer}, \tag{2}$$

where n is the period of the ground state in the field, S is the magnitude of the spin and m is the magnetization per site in units of $g\mu_B$. It is worth mentioning that n can be different from the period of the lattice. In this case, symmetry breaking is introduced at the magnetization plateau. However, most of the theoretical models considered so far in one dimension are cases without breaking of the translational symmetry [9–12]. To our knowledge, the first example where the ground state at plateau breaks the symmetry is the $S = 1/2$ Heisenberg model chain with next-nearest-neighbour and alternating nearest-neighbour interactions [14, 15]. In experiments, several one-dimensional spin systems have been synthesized [16–19]. One of them $[Ni_2(Medpt)_2(\mu\text{-ox})(\mu\text{-}N_3)]ClO_4{\cdot}0.5H_2O$ (Medpt = methyl-bis(3-aminopropyl)amine) is considered to be a realization of the $S = 1$ antiferromagnetic chain with bond alternation [20]. Actually a magnetization plateau is observed as predicted by theoretical calculations [11, 12]. However, this is an example of a case without breaking of the translational symmetry. So far, a plateau accompanied by symmetry breaking does not seem to have been found in one-dimensional materials.

Recently Kageyama *et al* [22] rediscovered a new two-dimensional spin gap system $SrCu_2(BO_3)_2$ [21]. The magnetic properties of this compound are carried by Cu^{2+} ions which may be well represented by localized spins of $S = 1/2$. The network of Cu^{2+} ions has a structure for which strong frustration effects are expected. In fact, this material shows various unique features:

Table 1. Spin gap Δ estimated from various experiments (NQR, nuclear quadrupole resonance; NMR, nuclear magnetic resonance; ESR, electron spin resonance).

Method	Spin gap
Magnetic susceptibility [23]	34 ± 1 K
Cu NQR, T_1 [22]	30 K
Magnetization curve [23]	22.5 T (31.3 K)
Cu NMR, Knight shift [29]	35 K
B NMR, T_1 [29]	36 K
Specific heat [30]	35.0 K
ESR [31]	722 GHz (34.7 K)
Neutron scattering [24]	3.0 meV (35 K)
Raman scattering [32]	24.5 cm^{-1} (35.2 K)
Far infrared spectroscopy [33]	24.2 cm^{-1} (34.8 K)

(i) *Spin-gapped behaviour.* The temperature dependence of the magnetic susceptibility is shown in figure 2 [23]. It has a maximum at around 20 K and rapidly drops toward zero with decreasing temperature. This suggests the existence of a spin gap. Kageyama *et al* [23] estimate the value of the spin gap to be $\Delta = 34 \pm 1$ K based on the fit to the isolated dimer model below 6 K. In addition to that, various experiments show the evidence that $SrCu_2(BO_3)_2$ has the spin gap $\Delta \sim 35$ K (table 1). Therefore it is experimentally confirmed that the ground state of this material is nonmagnetic.

(ii) *Unusual excitations.* The lowest branch of magnetic excitations has an almost localized nature, as will be explained in section 4. This character is observed as an almost flat dispersion in an inelastic neutron scattering experiment [24]. On the other hand, higher-energy excitations observed in neutron scattering experiments have a dispersive character. These excitations are also observed in electron spin resonance (ESR), Raman scattering and far infrared spectroscopy (see table 3 in section 4.2).

(iii) *Magnetization plateaux.* High-field magnetization measurements have been performed and $1/3$, $1/4$ and $1/8$ plateaux are observed [22, 25]. The results up to 69 T at 1.4 K are shown in figure 3 [26]. Symmetry breaking is expected at each plateau from theoretical studies (see section 6). Oshikawa has extended the argument in [13] to arbitrary dimensions and it is shown that the necessary condition for plateau (2) is still valid in arbitrary dimensions [27]. In fact, the plateaux theoretically obtained for the model of $SrCu_2(BO_3)_2$ satisfy the condition (2). Recently Kodama *et al* [28] have done a nuclear magnetic resonance (NMR) measurement up to 27 T and actually observed several nonequivalent spin sites existing at the $1/8$ plateau. To our knowledge, $SrCu_2(BO_3)_2$ is the first example of a two-dimensional material in which the ground state at plateau has a symmetry breaking.

Note that, in figure 3, even below the critical field, which is around 23 T, the magnetization is finite. Experimentally, it was checked that reducing the temperature does not affect the finite magnetization. Its origin is not yet clear.

Since the discovery of $SrCu_2(BO_3)_2$, many studies have been made by both experimentalists and theorists to elucidate these rich unusual magnetic properties.

In this article we review the development of research on $SrCu_2(BO_3)_2$ at the present stage from the theoretical point of view. This review is organized as follows. Firstly its crystal structure is shown and the orthogonal dimer model is presented. After that the ground state properties of this model are discussed in section 3. It has an exact dimer singlet ground state in some parameter ranges. The quantum phase transitions of the model are also discussed.

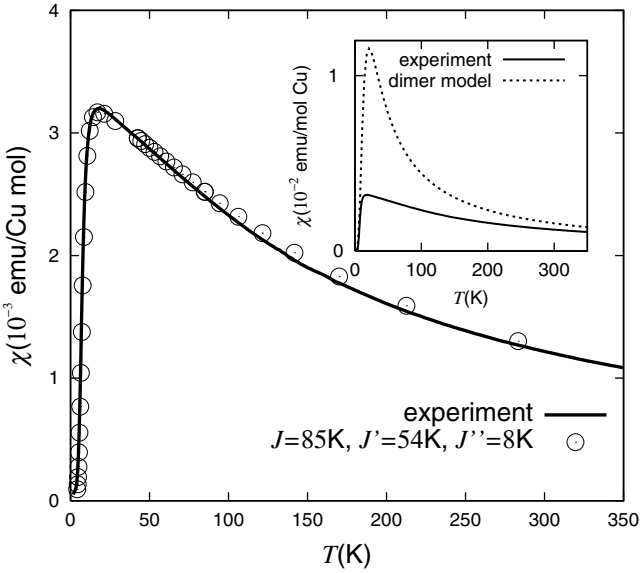

Figure 2. The temperature dependence of the magnetic susceptibility (solid curve). Circles are the result of numerical calculation with the optimal parameter set (see section 5). The inset is the result of fitting by an isolated dimer model.

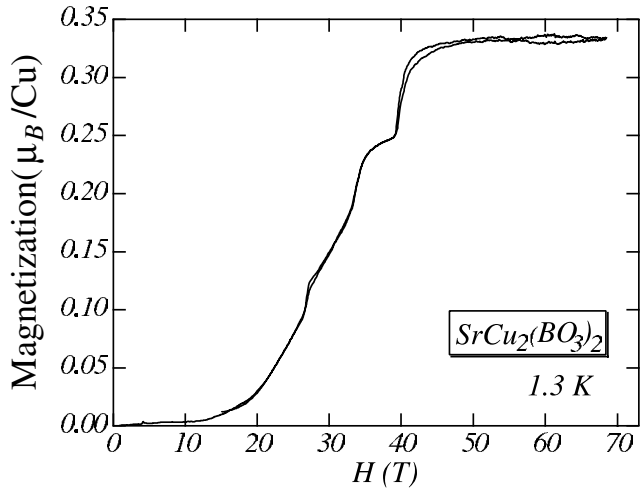

Figure 3. The magnetization curve for $SrCu_2(BO_3)_2$ at 1.3 K. The magnetic field is applied along the *c*-axis. 1/3, 1/4 and 1/8 plateaux are observed (reproduced from [26]).

In section 4, excited states are treated. The lowest branch of triplet excitations has an almost localized nature. On the other hand, two triplet excitations make a bound state and the combined excitations hop in the lattice more easily than the single triplet excitations. An estimation of the parameters of the model is made by comparing various quantities with experiments in section 5. The analysis indicates that the parameter set for $SrCu_2(BO_3)_2$ lies in the region where the exact ground state is realized. Finally, in section 6, properties of $SrCu_2(BO_3)_2$ in an external magnetic fields are discussed. In a magnetic field some of the singlets are promoted

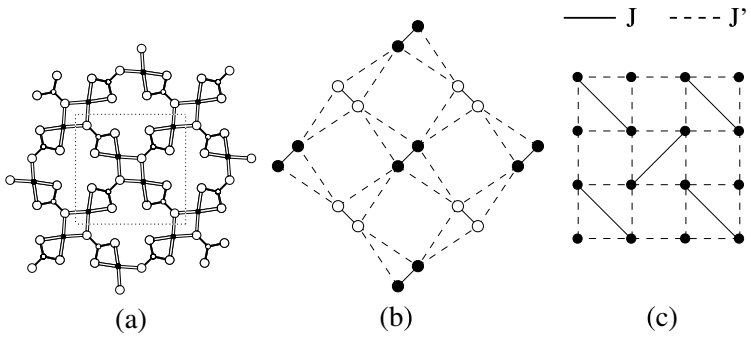

Figure 4. (a) Schematic view of the crystal structure of a $CuBO_3$ layer. Full circles represent Cu sites. Big open circles are O sites and small open circles B sites. The dotted line shows the unit cell (reproduced from [22]). (b) Two-dimensional orthogonal dimer model, which is equivalent to (c) the Shastry–Sutherland model. Below $T_s = 395$ K, a buckling of the $CuBO_3$ plane is observed. Dimers shown by white (black) dumbbells make a flat plane and the two planes are slightly shifted from each other.

to the triplet states. Because of their almost localized character, crystallization of triplets takes place at certain magnetizations, which leads to magnetization plateaux. In these plateaux, except for the 1/2 plateau, the symmetry of the ground state is lower than the symmetry of the original Heisenberg model. We discuss the possible superstructures at each plateau. Conclusions are summarized in section 7.

2. Orthogonal dimer models for $SrCu_2(BO_3)_2$

2.1. Crystal structure

The crystal structure of $SrCu_2(BO_3)_2$ is tetragonal and is characterized by a layered structure of $CuBO_3$ and Sr planes [21, 22, 34]. At room temperature, the lattice constants are $a = 8.995$ Å and $c = 6.649$ Å. A sketch of a $CuBO_3$ layer is shown in figure 4(a). In this layer BO_3 molecules make a triangle and Cu^{2+} ions are connected through the BO_3 molecules. All Cu^{2+} ions are located at crystallographically equivalent sites and have a spin $S = 1/2$. Each Cu^{2+} ion has one nearest-neighbour Cu^{2+} ion and four next-nearest-neighbour Cu^{2+} ions in the plane. The two-dimensional linkage of the Cu^{2+} ions is illustrated in figure 4(b). A pair of nearest-neighbour Cu^{2+} ions connected through O sites, which are vertices of BO_3 triangles, form a dimer unit. The dimer units are connected orthogonally through BO_3 molecules. The distance between the nearest-neighbour Cu^{2+} ions is 2.905 Å, and that between the next-nearest-neighbour Cu^{2+} ions is 5.132 Å at room temperature. A buckling of the $CuBO_3$ plane is observed below 395 K. The unit cell in the layer contains two types of dimer (white and black dumbbells in figure 4(b)) which are mutually orthogonal. One type of dimer makes a flat plane and the two planes are slightly shifted from each other. Projection of the dimer bonds along [110] at 100 K is illustrated in figure 5(a).

At $T_s = 395$ K, a structural phase transition from the space group $I\,\bar{4}\,2$ to $I\,4/m\,c\,m$ (both are tetragonal) has been observed by x-ray diffraction. Anomalies at T_s have been observed by Raman scattering, temperature dependence of the magnetic susceptibility, and differential scanning calorimetry measurements [34]. Above T_s, two dimers in the unit cell lies on the same plane (figure 5(b)) and there is no buckling of the $CuBO_3$ plane. Therefore the $CuBO_3$ plane is a mirror plane.

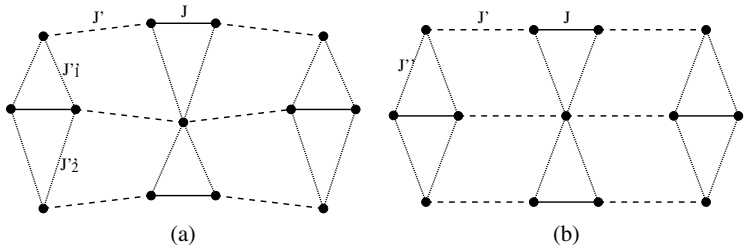

Figure 5. (a) A sketch of the projection of the dimer bonds along [110] at 100 K. There is a buckling of the $CuBO_3$ plane. Two types of interlayer interactions J_1'', J_2'' exist. (b) A sketch at 433 K. The $CuBO_3$ plane is a mirror plane.

The existence of a mirror plane is important for Dzyaloshinsky–Moriya interactions. Above T_s, the Dzyaloshinsky–Moriya interactions may exist only for the next-nearest-neighbour pairs and do not exist for the nearest-neighbour pairs since the middle of a nearest-neighbour bond is an inversion centre. On the other hand, below T_s, the mirror plane is lost. Therefore not only Dzyaloshinsky–Moriya interactions on the next-nearest-neighbour pairs but also those on nearest-neighbour pairs can exist. However, since the magnitude of the shift is small, the Dzyaloshinsky–Moriya interaction which exists above T_s may be considered to be the most important and other components may be ignored.

2.2. Two-dimensional orthogonal dimer model

The nearest-neighbour Cu^{2+} ions are connected through O^{2-} ions, where the bridging angle Cu–O–Cu is 102.42° at room temperature, and therefore it is reasonable to assume that the intradimer exchange interaction J is antiferromagnetic. From the crystal structure shown in figure 4(a), one may expect that the magnetic properties of $SrCu_2(BO_3)_2$ would be explained approximately by the isolated dimer. However, this model cannot describe the peculiar magnetic behaviour of this material, for example the presence of magnetization plateaux. Also the temperature dependence of the magnetic susceptibility of the isolated dimer model, where the unique parameter J is given by the magnitude of the spin gap of 35 K, is very different from the experimental results shown in the inset of figure 2: the observed peak is significantly suppressed [22]. The difference comes from the relatively large Curie–Weiss constant compared with the spin gap. The Curie–Weiss constant $\theta = 102.5$ K is estimated from fitting in the temperature range between 250 and 350 K [23]. This fact indicates the existence of a frustrated antiferromagnetic coupling J'.

Thus a two-dimensional Heisenberg model with the nearest-neighbour coupling J and the next-nearest-neighbour coupling J',

$$\mathcal{H} = J \sum_{\mathrm{nn}} \boldsymbol{s}_i \cdot \boldsymbol{s}_j + J' \sum_{\mathrm{nnn}} \boldsymbol{s}_i \cdot \boldsymbol{s}_j, \tag{3}$$

may be a good model for the magnetic properties of $SrCu_2(BO_3)_2$ (figures 4(b) and 6(a)). As we will show below, it describes well various magnetic properties of $SrCu_2(BO_3)_2$. In this model, the orthogonality between the two nearest-neighbour dimers plays an important role, as will be discussed below, and therefore we call it orthogonal dimer model [35]. The model is topologically equivalent to the Shastry–Sutherland model (shown in figure 4(c)). Shastry and Sutherland constructed the model in such a way as to realize an exact ground state [36]. Therefore the original Shastry–Sutherland model looks very artificial and it seems almost impossible to find a real material whose structure is represented by it. In fact, it took almost

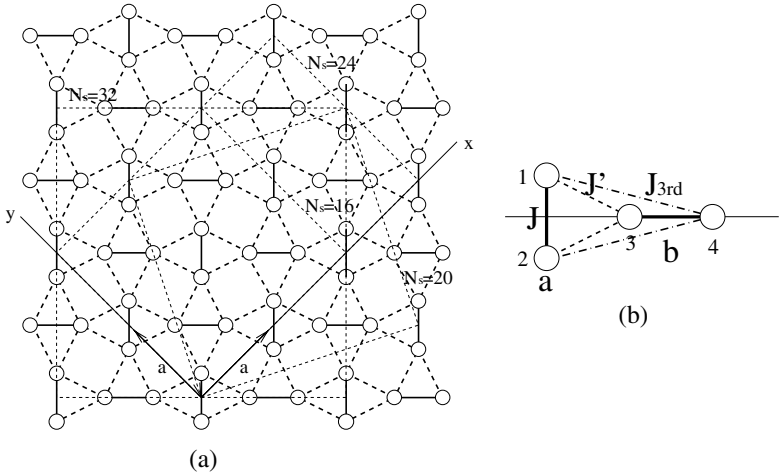

Figure 6. (a) Two-dimensional orthogonal dimer Heisenberg model. The lattice constant a is shown by arrows. Also shown are clusters for $N_s = 16, 20, 24, 32$ (dashed lines). (b) A unit bond for the orthogonal dimer model.

20 years to find a material which is a realization of the Shastry–Sutherland model. In this review, we use two names distinctively. In most cases we use the name 'the orthogonal dimer model'. However, when we use the name 'Shastry–Sutherland model', we imagine the square lattice structure with the diagonal bonds. Note that in the orthogonal dimer model the nearest-neighbour interaction is J, however, in the Shastry–Sutherland model, the nearest-neighbour interaction is J'.

2.3. Three-dimensional orthogonal dimer model

The three-dimensional structure of $SrCu_2(BO_3)_2$ consists of $CuBO_3$ layers and Sr layers as mentioned before. Above T_s, the $CuBO_3$ layers stack alternately and the magnetic ions of the $CuBO_3$ layers form a three-dimensional lattice structure shown in figure 7 [37], which may be represented by

$$\mathcal{H} = J \sum_{\text{nn}} \boldsymbol{s}_i \cdot \boldsymbol{s}_j + J' \sum_{\text{nnn}} \boldsymbol{s}_i \cdot \boldsymbol{s}_j + J' \sum_{il} \boldsymbol{s}_i \cdot \boldsymbol{s}_j. \tag{4}$$

In addition to the intraplane interactions J and J', an interlayer interaction J'' is introduced. The Cu^{2+}–Cu^{2+} distance for the J'' bond is shorter than that of the next-nearest-neighbour bond in each plane. However, we expect that J' is much bigger than J'' since the dominant path of the super-exchange of J' is through the molecular orbital of BO_3 and, on the other hand, the Sr^{2+} ion has a closed shell.

Below T_s, there is a buckling in the $CuBO_3$ plane and thus the distances between Cu^{2+} ions of the adjacent dimers are 3.593 or 4.233 Å at room temperature. In this way, strictly speaking, there are two types of interlayer coupling: J''_1 and J''_2 (see figure 5). However, the difference hardly affects the magnetic properties of $SrCu_2(BO_3)_2$, as will be shown in sections 3.1.2, 4.1 and 5. For simplicity we will use the same coupling constant for both.

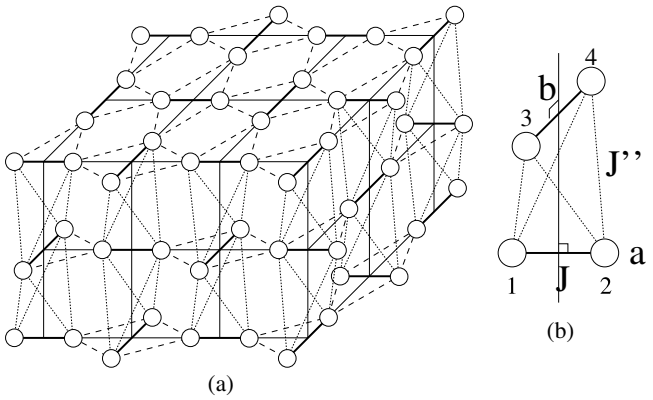

Figure 7. (a) Three-dimensional orthogonal dimer model for $SrCu_2(BO_3)_2$. (b) A configuration of orthogonal dimers along the c direction.

3. Ground states of orthogonal dimer models

3.1. Exact dimer singlet ground state

3.1.1. Two-dimensional orthogonal dimer model for $SrCu_2(BO_3)_2$. The most remarkable property of the Hamiltonian (3) is that the direct product of the singlet states on J bonds

$$|\Psi\rangle = \prod_a |s\rangle_a = \prod_a \frac{1}{\sqrt{2}}(|\uparrow\downarrow\rangle_a - |\downarrow\uparrow\rangle_a) \tag{5}$$

is always an eigenstate. In the above equation, a denotes a nearest-neighbour bond. In the case $J' = 0$, obviously it is a ground state with energy $E_g/N_s = -3/8$ J and spin gap J and therefore it is expected that equation (5) is the ground state for $J'/J \ll 1$. The exact ground state was pointed out first by Shastry and Sutherland over 20 years ago [36, 38]. The exact dimer singlet state is also realized in a zig-zag spin chain model but this is true only at the fully frustrated point $J_1 = 2J_2$ [4]. Another difference between the present case and the Majumdar–Ghosh model is that the translational symmetry is broken in the latter case while it is preserved in the former.

The proof for the exact eigenstate is simple. Let us consider the effect of the second term of the Hamiltonian (3), since the wavefunction (5) is an eigenstate, actually the ground state, of the first term. It is easy to show by elementary calculations that for any neighbouring pair of the nearest-neighbour bonds a ket to which operator $\mathcal{H}'_{ab}$ is applied vanishes:

$$\mathcal{H}'_{ab}|s\rangle_a|s\rangle_b = 0. \tag{6}$$

To be explicit, $\mathcal{H}'_{ab} = J'(\boldsymbol{s}_1 \cdot \boldsymbol{s}_3 + \boldsymbol{s}_2 \cdot \boldsymbol{s}_3)$ where the site indices are defined in figure 6(b). Note that the vanishing of the ket is due to the difference in parity between the singlet and the triplet, odd and even, with respect to the reflection which exchanges the two spins $\boldsymbol{s}_1 \leftrightarrow \boldsymbol{s}_2$. For the orthogonal configurations the Hamiltonian conserves the parity. On the other hand when a spin operator is applied to a singlet, a finite matrix element is possible only for some component of the triplet. These requirements are in contradiction. Therefore all matrix elements should vanish.

Next let us prove that equation (5) is the ground state for some parameter range. Here we follow the method used by Shastry and Sutherland [36]. The Hamiltonian (3) can be considered as a sum of triangles, which are written as $\mathcal{H}_t = J/2(\boldsymbol{s}_1 \cdot \boldsymbol{s}_2) + J'(\boldsymbol{s}_1 \cdot \boldsymbol{s}_3 + \boldsymbol{s}_2 \cdot \boldsymbol{s}_3)$. The

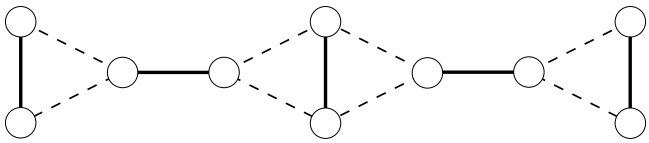

Figure 8. One-dimensional orthogonal dimer model with interdimer couplings J' (reproduced from [37]).

ground state energy of each triangle is $e_t = -3/8$ J for $J'/J \leqslant 0.5$ and $e_t = J/8 - J'$ for $J'/J \geqslant 0.5$. By using these results, the ground state energy is estimated as $e_t N_t$, where N_t is the number of triangles. Since the ground energy $e_t N_t$ is estimated by a variational calculation, the actual ground state energy of the Hamiltonian (3) E_g satisfies the condition $e_t N_t \leqslant E_g$. For $J'/J \leqslant 0.5$, $e_t N_t$ is equal to the eigenvalue of the eigenstate (5). Thus the state (5) is the ground state in this parameter range. On the other hand, for $J'/J > 0.5$, the model has not been solved exactly. This fact indicates that the real phase transition point should be bigger than $(J'/J)_c = 0.5$. In fact, a series expansion calculation by Koga and Kawakami [39] gives the phase transition point $(J'/J)_c = 0.68$. Details of the estimation of the phase transition point $(J'/J)_c$ will be discussed in section 3.2.1.

3.1.2. Three-dimensional orthogonal dimer model for $SrCu_2(BO_3)_2$. A three-dimensional model for $SrCu_2(BO_3)_2$ is written as equation (4) [37]. In this model, the dimer singlet state (5) is still an eigenstate since the kets to which operators for interlayer coupling J'' are applied vanish:

$$J''(\boldsymbol{s}_1 + \boldsymbol{s}_2) \cdot (\boldsymbol{s}_3 + \boldsymbol{s}_4)|s\rangle_a|s\rangle_b = 0 \tag{7}$$

where the site indices are shown in figure 7(b). It is clear that the dimer singlet state is the ground state for small J'/J and J''/J. This result remains true even if we include the alternation along the c-axis: J_1'' and J_2'' (see figure 5(a)).

It is expected that the interlayer interactions are smaller than J and J' and the two-dimensional orthogonal dimer model is a good starting point for $SrCu_2(BO_3)_2$. However, the exactness of the dimer singlet ground state for the three-dimensional model is one of the reasons why magnetic properties of $SrCu_2(BO_3)_2$ are well described by the two-dimensional model.

3.1.3. A class of orthogonal dimer models with an exact dimer singlet ground state. So far several orthogonal dimer models have been considered in the literature. In such a model, the exact dimer singlet ground state (5) may be realized because of the orthogonality of the dimer bonds. In this section, we will discuss a class of orthogonal dimer models which are related to $SrCu_2(BO_3)_2$.

We start our discussion with two examples in one dimension. The one-dimensional version of the orthogonal dimer model considered for $SrCu_2(BO_3)_2$ is shown in figure 8, where the bonds denoted by the thick solid lines define a unique covering of the spins and the broken lines are the bonds connecting dimers. We use J for the coupling constant in the dimers and J' for the interdimer couplings. For this model the dimer singlet state is an exact eigenstate for any J'/J and the ground state for small J'/J [37, 40, 41]. This is easily proven from equation (6). The result holds independent of the magnitude of the spin, S. For example, the ground states for arbitrary S are studied by Koga and Kawakami [42].

In the model of figure 8, the neighbouring dimers are orthogonal but in the same plane. On the other hand, another one-dimensional Heisenberg model with the exact dimer ground state

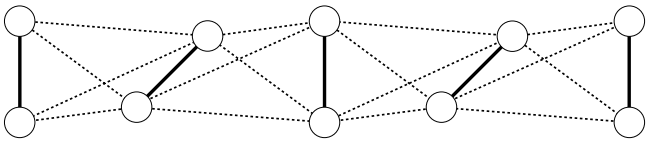

Figure 9. One-dimensional orthogonal dimer model with inter dimer couplings J''. The model is topologically equivalent to the spin ladders with diagonal couplings (reproduced from [37]).

may be constructed by making one type of dimer out of the plane (figure 9). The bonds between the orthogonal dimers of this type are defined as J'' bonds in figure 9. As shown in figure 7(a), in $SrCu_2(BO_3)_2$ the dimers along the c-axis are coupled as in this model. It is straightforward to confirm that all matrix elements of the J'' bonds vanish as already discussed (equation (7)). The present model is topologically equivalent to the spin ladders with the diagonal couplings of the same amplitude to the couplings of the legs discussed in [37, 43].

It is obvious that any combination of the two types of orthogonal dimer may have the dimer singlet state as the exact eigenstate. This is still possible in two- or three-dimensional models as long as the neighbouring dimers are orthogonal [37, 44, 45]. For example, the regularly depleted orthogonal dimer models [37] and two types of three-dimensional orthogonal dimer model [44, 45], whose lattices are different from that for $SrCu_2(BO_3)_2$, have been considered. The lattice structures of each model are shown in these references.

Another type of model is possible with even longer-range interactions. For example, the two-dimensional orthogonal dimer model with the interaction J_{3rd} shown in figure 6(b) was proposed by Weihong *et al* [46] and Müller-Hartmann *et al* [47] and it also has the exact dimer singlet ground state for small J' and J_{3rd}.

3.2. Quantum phase transitions of the orthogonal dimer models

3.2.1. Two-dimensional orthogonal dimer model. In this section we discuss quantum phase transitions of the two-dimensional Shastry–Sutherland model. For small J'/J, the exact dimer singlet state discussed in the previous section is the ground state. It has a spin gap and does not have long-range order. On the other hand, given $J = 0$ and $J' \neq 0$, the model is equivalent to a two-dimensional square lattice Heisenberg model (see figure 4(c)). For the two-dimensional Heisenberg model, there is a consensus that the ground state has antiferromagnetic long-range order and no spin gap [48]. It means that the antiferromagnetically ordered state should be the ground state for some parameter $J'/J \gg 1$. In addition to these two states, the possibility of the existence of other states between the dimer singlet state and the antiferromagnetically ordered state was pointed out [39, 49]. Motivated by these works, several subsequent works have been published. The proposed phase transition points are summarized in table 2. Initially, a direct phase transition from the dimer singlet state to the antiferromagnetically ordered state was proposed [35, 46]. But recent works favour the possibility of an intermediate phase, which is now thought likely to exist. At this stage, two possible intermediate phases have been proposed: helical order [49, 50] and plaquette resonating-valence-bond [39, 51, 52].

(1) Helical ordered state. As discussed by Shastry and Sutherland, it is known that in the classical limit, when $S \to \infty$, the ground state has helical order for $J'/J > 1$ and Néel order otherwise (details for the classical case are discussed in [36, 49]). Therefore it may seem natural to expect a helical ordered ground state even for $S = 1/2$. From such a point of view, Albrecht and Mila studied the stability of the helical ordered state [49]. They have investigated

Table 2. Phase boundary points calculated by several theories. A dash means that there is no intermediate phase transition. The phase transition is also discussed in [50] (large-N limit of the Sp(N) Shastry–Sutherland model) and [53] (field theory approach for generalized Shastry–Sutherland models). Since the model is generalized in both methods, we have not included their results in the table.

Main method	$(J'/J)_{c1}$	$(J'/J)_{c2}$	Intermediate phase
Variational method [36]	0.5	—	—
Schwinger boson mean field theory [49]	0.6	0.9	Helical ordered state
Exact diagonalization (up to 20 sites) [35]	0.70(1)	—	—
Ising expansion [46]	0.691(6)	—	—
Dimer expansion [47]	0.697(2)	—	—
Plaquette expansion [39]	0.677(2)	0.86	Plaquette singlet
Series expansion [54]	0.69	0.83 or —	Columnar or —
Exact diagonalization (up to 32 sites) [52]	0.67	Bigger than 0.71	Plaquette singlet

the stability of both the helical and the Néel ordered states by Schwinger boson mean-field theory.

In the Schwinger boson mean-field theory, the spin operators $\boldsymbol{s}_i$ are replaced by bosonic operators $b^\dagger_{i\sigma}\sigma_{\sigma\sigma'}b_{i\sigma'}/2$ with a constraint on the number of particles on each site $b^\dagger_{i\uparrow}b_{i\uparrow} + b^\dagger_{i\downarrow}b_{i\downarrow} = 2S$ to fix the size of the spin. The Hamiltonian (3) is rewritten by using the bosonic operators $2A^\dagger_{ij} = b^\dagger_{i\uparrow}b^\dagger_{j\downarrow} + b_{i\downarrow}b_{j\uparrow}$ and $2B^\dagger_{ij} = b^\dagger_{i\uparrow}b_{j\uparrow} + b^\dagger_{i\downarrow}b_{j\downarrow}$:

$$\mathcal{H} = \sum_{(i,j)} J_{ij}(:B^\dagger_{ij}B_{ij}: - A^\dagger_{ij}A_{ij}), \tag{8}$$

where $:A:$ is a normal ordered operator in which annihilation operators are moved to the right. Introducing the order parameters $\alpha_{ij} = \langle A^\dagger_{ij}\rangle/2$ and $\beta_{ij} = \langle B^\dagger_{ij}\rangle/2$, the Hamiltonian at mean-field level is written:

$$\mathcal{H}_{MF} = \sum_{(i,j)} J_{ij}(\beta_{ij}(B_{ij} + B^\dagger_{ij}) - \alpha_{ij}(A_{ij} + A^\dagger_{ij}) - \beta^2_{ij} + \alpha^2_{ij}) \tag{9}$$

$$+ \mu \sum_i (b^\dagger_{i\uparrow}b_{i\uparrow} + b^\dagger_{i\downarrow}b_{i\downarrow} - 2S). \tag{10}$$

The last term (equation (10)) with chemical potential μ is added to satisfy the local constraint, which is replaced by a global one in the present scheme, and plays the role of a Lagrange parameter. To treat the helical ordered state one has to multiply each Bose operator by a phase factor $\exp(\mathrm{i}\boldsymbol{Q}\cdot\boldsymbol{r}_i/2)$, where $\boldsymbol{Q}$ is the pitch of the helix. The order parameters are given by

$$\alpha_{ij} = \exp(-\mathrm{i}\boldsymbol{Q}\cdot\boldsymbol{r}_i/2)\langle b^\dagger_{i\uparrow}b_{j\uparrow}\rangle + \exp(\mathrm{i}\boldsymbol{Q}\cdot\boldsymbol{r}_i/2)\langle b^\dagger_{i\downarrow}b_{j\downarrow}\rangle, \tag{11}$$

$$\beta_{ij} = \exp(\mathrm{i}\boldsymbol{Q}\cdot\boldsymbol{r}_i/2)\langle b_{i\uparrow}b_{j\downarrow}\rangle - \exp(-\mathrm{i}\boldsymbol{Q}\cdot\boldsymbol{r}_i/2)\langle b_{i\downarrow}b_{j\uparrow}\rangle, \tag{12}$$

$$2S = \langle b^\dagger_{i\uparrow}b_{j\uparrow}\rangle\langle b^\dagger_{i\downarrow}b_{j\downarrow}\rangle. \tag{13}$$

These equations define a system of self-consistent nonlinear equations for α_{ij} and β_{ij} since the expectation values $\langle b^\dagger_{i\sigma}b_{j\sigma}\rangle$ and $\langle b_{i\sigma}b_{j\sigma}\rangle$ can be calculated from equation (10). Long-range order is described by a Bose condensation. The solutions of these equations for an arbitrary value of $\boldsymbol{Q}$ and a given value of S lead to an excitation spectrum which is gapless at three points of the Brillouin zone located at $\boldsymbol{k} = (\boldsymbol{Q} - \boldsymbol{Q}_0)/2$ and $(\boldsymbol{Q} - \boldsymbol{Q}_0)/2 \pm \boldsymbol{Q}_0$, where $\boldsymbol{Q}_0$ depends on S and J/J' but not on $\boldsymbol{Q}$. By choosing $\boldsymbol{Q} = \boldsymbol{Q}_0$, a solution with a Goldstone mode at $\boldsymbol{k} = 0$ is obtained. By looking at the solution of the mean-field equations, where the Bose condensation occurs and the excitation spectrum is softened, the critical value for the magnitude of spin S is given. The results are shown in figure 10. The transition between Néel and helical order is

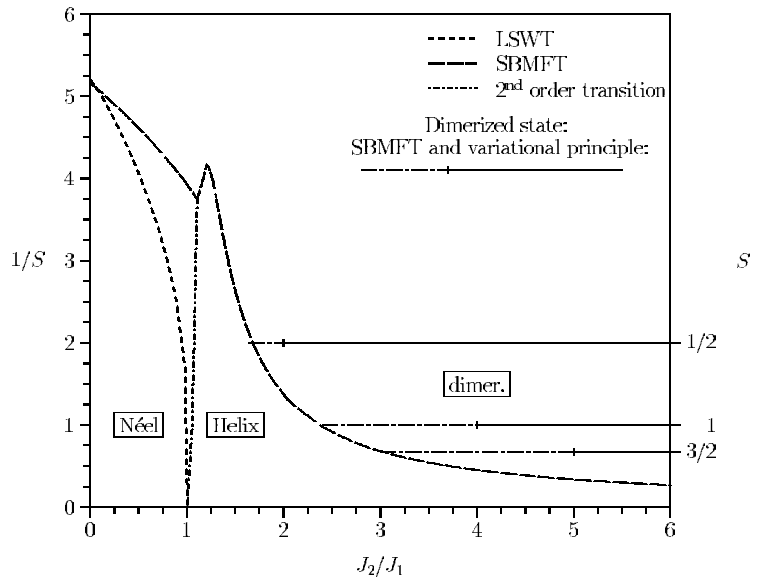

Figure 10. Phase diagram obtained by the Schwinger boson mean-field theory and the linear spin-wave theory. In this figure J_1 and J_2 mean J' and J (reproduced from [49]).

a second-order transition and the phase transition point for $S \to \infty$ is consistent with that of the classical model.

Recent gauge-theoretic analysis of the Shastry–Sutherland lattice with Sp $(2N)$ symmetry in the large N limit also indicates the existence of the helical order state as the intermediate phase; details of the calculation are discussed in [50].

Finally, we mention the results of the linear spin wave theory. In many cases, the spin wave theory gives a reasonable result when the ground state is magnetically ordered. In fact, Albrecht and Mila studied the stability of the ordered state using it (results are in figure 10). However, it has turned out that the helical phase is unstable for any finite but arbitrary large value of S, in contradiction to the results of the classical limit. That is the reason why they used the Schwinger boson mean field theory. The details of the linear spin wave theory and the reason for the instability of the helical order using this method are discussed in [49].

(2) Plaquette singlet state. Let us discuss another possible intermediate phase: the plaquette singlet state. Here we follow the argument presented by Koga and Kawakami [39]. The Hamiltonian on the Shastry–Sutherland lattice may be divided into three parts (figure 11(a)):

$$\mathcal{H} = J \sum_{\langle \mathrm{nnn} \rangle} \boldsymbol{s}_i \cdot \boldsymbol{s}_j + J_1' \sum_{\langle \mathrm{nn} \rangle'} \boldsymbol{s}_i \cdot \boldsymbol{s}_j + J_2' \sum_{\langle \mathrm{nn} \rangle''} \boldsymbol{s}_i \cdot \boldsymbol{s}_j, \tag{14}$$

where $\langle \mathrm{nn} \rangle'$ ($\langle \mathrm{nn} \rangle''$) means that the sum runs over on the nearest-neighbour sites presented by the thin (dashed) lines in the figure. The lattice is invariant under the exchange of J_1' and J_2'. Therefore only the case $J_1' \geqslant J_2'$ is discussed. As shown in figure 11, the Shastry–Sutherland model is topologically equivalent to the 1/5-depleted square lattice, which was used for CaV_4O_9 [55, 56].

In this generalized model, Koga and Kawakami analysed the ground state properties based on the plaquette expansion, where the J_1' term is the unperturbed part and the J and J_2' terms are treated as perturbations. The ground state of the unperturbed Hamiltonian is the

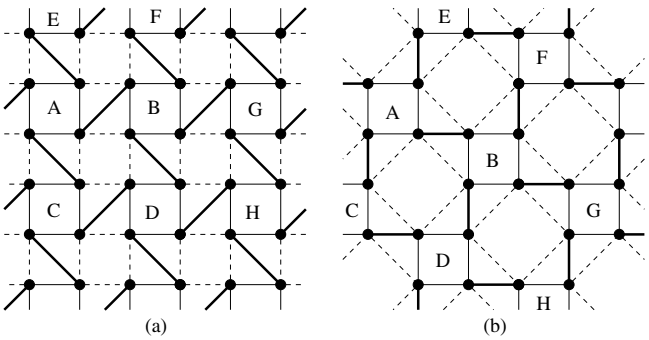

Figure 11. Two-dimensional system with plaquette structure. Thick, thin, dashed lines represent the coupling constants J, J_1' and J_2' in equation (14). (a) On the Shastry–Sutherland lattice. (b) On the 1/5-depleted square lattice. Letters correspond to the equivalent plaquette on each lattice.

product of plaquette singlets with a spin gap. They calculated the staggered susceptibility χ_{AF}, the spin gap energy Δ at $\boldsymbol{k} = (0, 0)$ and the ground state energy E_g as a power series in J and J_2', where the ratio J_2'/J was kept as a constant value α. The Zeeman term under the staggered magnetic field was introduced to calculate the staggered susceptibility. The staggered susceptibility and the spin gap up to fourth and fifth order in J and J_2' have been calculated for various values of α. Using Padé approximants (both the Dlog and the biased Padé approximants), the phase transition points between the gapless magnetically ordered state and the gapped disordered state (plaquette singlet state) are estimated and results are shown in figure 12. Here the critical values of J_2'/J_1' are determined by using the formula $\chi_{AF} \sim ((J_2'/J_1')_c - J_2'/J_1')^{\gamma}$ and $\Delta \sim ((J_2'/J_1')_c - J_2'/J_1')^{\nu}$ with the known values $\gamma = 1.4$ and $\nu = 0.71$ for the universality class of the three-dimensional classical Heisenberg model, to which two-dimensional quantum spin models should belong [57]. For $J_2'/J_1' = 1$, the critical value $(J'/J)_{c2} = 0.86(1)$ is obtained from the spin gap determined by means of the biased Padé approximants. This fact indicates that the Shastry–Sutherland model has a disordered ground state in the region $J'/J < (J'/J)_{c2}$. On the other hand, for small J'/J, the ground state on the Shastry–Sutherland model is described by the product of the dimer singlets. In this phase, the dimer expansion indicates that the spin gap vanishes around $J'/J = 0.7$ [46, 47], which is smaller than $(J'/J)_{c2} = 0.86(1)$. This fact may point to the existence of a quantum phase transition from the dimer singlet ground state to the plaquette singlet ground state.

Koga and Kawakami also calculated the ground state energy for the plaquette singlet ground state by performing a plaquette expansion up to seventh order in J and J_2' keeping their ratio J_2'/J constant, and they estimated the ground state energy for the Shastry–Sutherland model by the first-order inhomogeneous differential method. Comparison of the ground state energy of the plaquette singlet state with that of the dimer singlet state energy $-3/8JN$ gives the critical point $(J'/J)_{c1} = 0.677(2)$. From the ground state energies obtained by the plaquette and Ising [46] expansions, the phase transition point between the disordered state and the ordered state $(J'/J)_{c2}$ is also estimated and the result is consistent with the value estimated from the spin gap and staggered susceptibility.

Takushima *et al* [51] extended the series expansion of the Hamiltonian (14) for the general case, which includes the 1/5-depleted square-lattice model, and they found that the resonating plaquette singlet state of the Shastry–Sutherland model was adiabatically connected to the plaquette phase known for the 1/5-depleted square-lattice model. In addition to that, they performed the series expansion from the orthogonal dimer chain (figure 8) and showed that

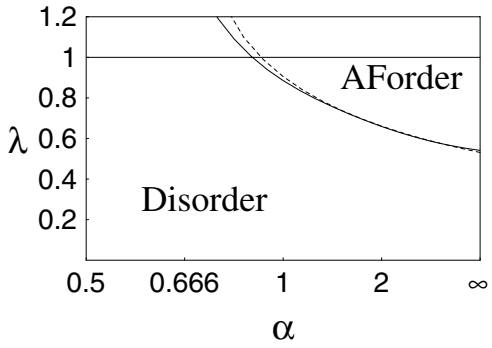

Figure 12. Phase boundary between the disordered and ordered state in the two-dimensional spin system on Shastry–Sutherland lattice. Here $\alpha = J_2'/J$ and $\lambda = J_2'/J_1'$. The line at $\lambda = 1$ corresponds to Shastry–Sutherland model. The solid (dashed) curve is the phase boundary estimated by a biased Padé approximation for the spin gap (the staggered susceptibility) (reproduced from [39]).

the plaquette phase of the Shastry–Sutherland model was adiabatically connected also to the plaquette phase of the orthogonal dimer chain. A recent calculation by Läuchli *et al* [52] using the dimer- and quadrumer-boson methods in the Shastry–Sutherland lattice also indicates that the intermediate state is connected to the plaquette phase of the 1/5-depleted square-lattice model [52]. These authors also performed an exact diagonalization for a cluster up to 32 sites and concluded in favour of the existence of the plaquette singlet state from the analysis of spin–spin correlation function.

On the other hand, Weihong *et al* [54] proposed the possibility that the plaquette-singlet phase is unstable. Their series expansion for the spin gap indicates that the minimum gap is no longer at $\boldsymbol{k} = (0, 0)$ for $J'/J \leqslant 0.8$ and $J_2'/J_1' \sim 1$ and their series expansion for $J'/J = 0.714$ suggests that the spin gap $\Delta(\pi/4, 3\pi/16)$ vanishes at $J_2'/J_1' = 0.998$. Comparing the ground state energies calculated by series expansions, they concluded that the Néel ordered state or the columnar state, as in the J_1–J_2 Heisenberg model, are possible ground states in the intermediate phase. Although the ground state energies of the Néel state or the columnar state are lower than that of the plaquette singlet state in their calculation, the difference is very small and the results might be different if the order of the calculations is changed. Also, Knetter *et al* [58] claimed that the instability of the two-magnon excitation might occur at $J'/J = 0.630(5)$ and this would indicate a transition to another phase at much lower values of J'/J than found before. But it is not clear whether this is evidence for the existence of another phase.

So, there are still open questions regarding the intermediate phase of the Shastry–Sutherland model but it seems to be reasonable to think that the disordered ground state, probably the plaquette singlet state, is stabilized by geometrical frustration.

At present our picture of the ground state of the orthogonal dimer model is the following. There may be three phases. The existence of the dimer singlet state and an antiferromagnetically ordered state is established. The nature of the intermediate state in this model still remains an open question. However, there is some evidence in favour of the existence of the plaquette resonating-valence-bond state. The helical ordered state remains a possibility based only on a crude approximation. To draw a definitive conclusion more elaborate treatments are necessary.

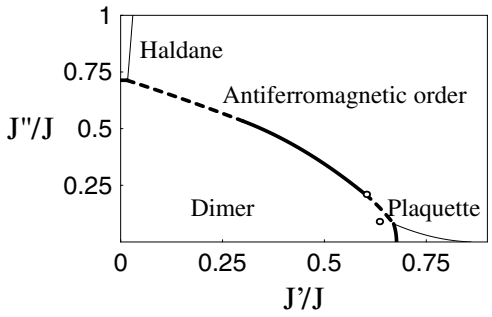

Figure 13. A phase diagram for the three-dimensional orthogonal dimer model. The circles reveal the parameter sets proposed for $SrCu_2(BO_3)_2$: $J'/J = 0.635$ and $J''/J = 0.09$ [60] and $J'/J = 0.603$ and $J''/J = 0.21$ [58] (reproduced from [59]).

3.2.2. Three-dimensional orthogonal dimer model. The phase diagram for the three-dimensional orthogonal dimer model (4) has been discussed only by the series expansion methods [59]. Koga has done plaquette (figure 11), coupled two-leg ladders $J' = 0$ (figure 9), and Ising expansions. The results are summarized in figure 13. The plaquette singlet phase (a frustration-induced disordered phase) is destroyed by small interlayer couplings J'' in contrast to the two-dimensional system.

As will be discussed in section 5, the estimated coupling constants for $SrCu_2(BO_3)_2$ are $J'/J = 0.635$ and $J''/J = 0.09$ [60]. These parameters show that $SrCu_2(BO_3)_2$ is located in the dimer phase close to the phase boundary between the dimer phase and the antiferromagnetically ordered phase. Substitutions of Ba or Ca ions for Sr ions or measurements under various pressures have been tried with the hope that these effects might change the interlayer couplings J'' and lead to the appearance of the antiferromagnetically ordered phase [26, 61]. But so far such a phase transition has not been observed.

4. Excitations

In this section, excited states in $SrCu_2(BO_3)_2$, i.e. excitations from the dimer singlet ground state, are discussed. The most significant feature of a triplet excitation is its almost localized character, which leads to the appearance of magnetization plateaux (see section 6). On the other hand, the bound states of two triplet excitations can move much more easily than an isolated triplet. These facts explain the unusual properties of the excitations observed in inelastic neutron scattering experiments and other methods.

4.1. The almost localized nature of a triplet

Let us consider the spin gap in the dimer singlet phase by using the perturbation theory ($J'/J < 1$) [35]. The spin gap up to the fourth-order correction is given by

$$\Delta = J\left(1 - \left(\frac{J'}{J}\right)^2 - \frac{1}{2}\left(\frac{J'}{J}\right)^3 - \frac{1}{8}\left(\frac{J'}{J}\right)^4\right). \tag{15}$$

One can show that up to the fifth order, the triplet excitation is completely localized.

This unusual behaviour is understood by considering the kets for triplet excitations to which operators are applied. To be explicit we consider the elementary unit shown in figure 6(b). There are two cases: a triplet is either on the vertical bond a or the horizontal bond b. The

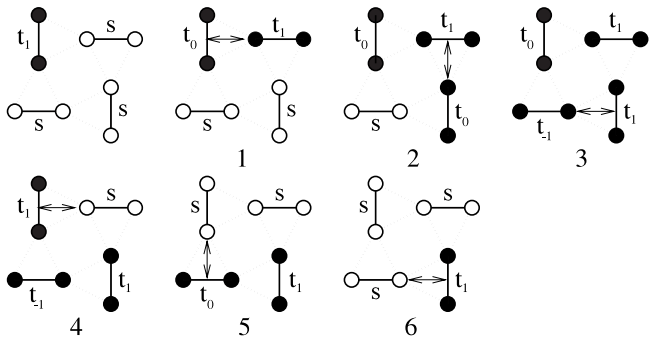

Figure 14. One of the lowest-order hopping processes of a triplet excitation. The triplet excitations hop to the next-nearest-neighbour dimer in sixth order of the perturbation.

matrix elements for the former case are

$$\mathcal{H}'_{ab}|t_m\rangle_a|s\rangle_b = \frac{J'}{2}|t_m\rangle_a|t_0\rangle_b - \frac{J'}{2}|t_0\rangle_a|t_m\rangle_b \qquad (m = \pm 1), \tag{16}$$

$$\mathcal{H}'_{ab}|t_0\rangle_a|s\rangle_b = \frac{J'}{2}|t_1\rangle_a|t_{-1}\rangle_b - \frac{J'}{2}|t_{-1}\rangle_a|t_1\rangle_b, \tag{17}$$

where $\mathcal{H}'_{ab} = J'(\boldsymbol{s}_1 \cdot \boldsymbol{s}_3 + \boldsymbol{s}_2 \cdot \boldsymbol{s}_3)$ and the site indices are shown in figure 6(b). $|t_m\rangle$ represents an $S^z = m$ triplet state. It is important to note that when a triplet moves to neighbouring bonds, it leaves another triplet behind because the parity on bond a is conserved from the reflection symmetry of the Hamiltonian (3). The next crucial observation is that all kets for the case where a triplet exists on bond b vanish by symmetry due to parity with respect to the reflection,

$$\mathcal{H}'_{ab}|s\rangle_a|t_m\rangle_b = 0 \qquad (m = 0, \pm 1). \tag{18}$$

The above facts, equations (16)–(18), set a stringent constraint for the motion of a triplet: hopping of the triplet is allowed only through forming a closed path of triplets. Otherwise, a trail of motion of a triplet is left behind. The lowest-order hopping process starts from the sixth order in the perturbation through such a closed path, as shown in figure 14.

The dispersion of the triplet excitation was calculated by series expansion [46, 58, 62] and exact diagonalization [63]. The results for the optimal set of parameters for $SrCu_2(BO_3)_2$ (see section 5) with both methods are shown in figure 15 [63, 64]. Here the almost localized nature of the triplet excitations is observed as an extremely narrow dispersion. In fact, such an almost flat band has been observed by inelastic neutron scattering [24], in agreement with the results of calculations. The band width estimated from the series expansion, 2.02 K (0.174 meV) [64], is consistent with the value observed in experiment, 2 K (0.2 meV) [24]. The dispersion is a minimum at $\boldsymbol{k} = (0, 0)$ and a maximum at $\boldsymbol{k} = (\pi, 0)$. Note that, as shown in figure 15, both results are consistent with each other and this fact indicates that both series expansion and finite size calculation are quite good approximations even for rather large parameters $J'/J = 0.635$.

Finally, let us consider the effects of two possible small interactions to the spin gap. One is the interlayer coupling J'' [60] and the other is the Dzyaloshinsky–Moriya interaction [65, 66]. These interactions may be small and may be treated by perturbation calculations. However, they play important roles in explaining the fine structure of the excited triplets:

(1) Effect of the interlayer coupling. In the case when one singlet bond is transformed into a triplet, the kets to which operators of the interlayer coupling J'' are applied vanish completely:

$$J''(\boldsymbol{s}_1 + \boldsymbol{s}_2) \cdot (\boldsymbol{s}_3 + \boldsymbol{s}_4)|t_m\rangle_a|s\rangle_b = 0 \qquad (m = 0, \pm 1). \tag{19}$$

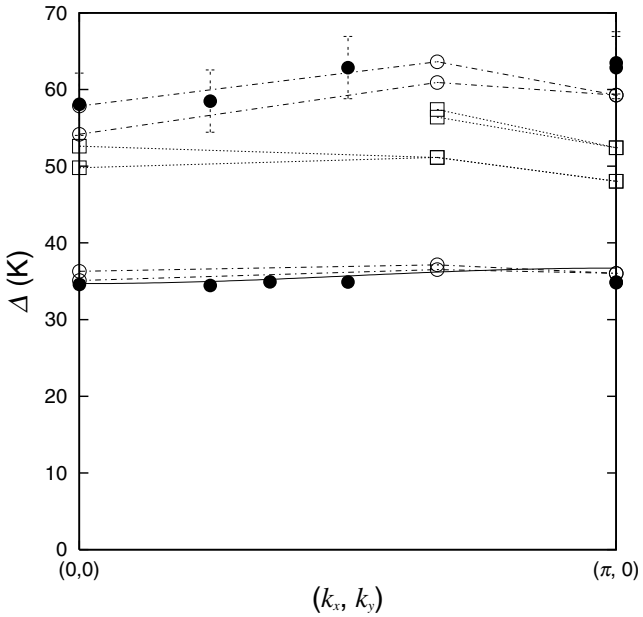

Figure 15. The dispersion relations for the excited states. The results of exact diagonalization for $J = 85$ K, $J'/J = 0.635$ and $N_s = 24$ are shown by open symbols. The active modes for neutron scattering are presented by open circles [63]. The results of the inelastic neutron scattering experiments are shown by full circles [24]. The solid line around 35 K is the result of the truncated dimer expansion by Weihong *et al* [46]: $J = 85$ K and $J'/J = 0.635$ are used.

Here the site indices are shown in figure 7(b). Thus the magnitude of the spin gap for the three-dimensional model does not change from the two-dimensional one. The dispersion of the triplet excitations is not modified, either. These facts mean that the properties of $SrCu_2(BO_3)_2$ can be well explained by using the two-dimensional orthogonal dimer model at low temperatures: $T < \Delta$, even in the presence of interlayer couplings.

There is an interaction effect in the case where triplets exist on both the a and b dimers in figure 7(b). Such a case is possible only when more than one triplet is excited. So the interlayer interaction J'' may affect the magnetic behaviours of $SrCu_2(BO_3)_2$ at high temperatures $T > \Delta$ or in high magnetic fields. In fact, to reproduce the temperature dependence of the magnetic susceptibility at $T > \Delta$, the inclusion of J'' is necessary [60].

(2) Effect of the Dzyaloshinsky–Moriya interaction. Anisotropic behaviour of the first excited state, which depends on the direction of the external field, was observed by ESR [31] and inelastic neutron scattering experiments [65]. A splitting of the spin gap energy was also observed in these experiments. These behaviours are qualitatively and semiquantitatively explained by considering the Dzyaloshinsky–Moriya interaction [65, 66]. Assuming that the $CuBO_3$ plane is a mirror plane, there is an inversion symmetry at the centre of the J bonds and Dzyaloshinsky–Moriya interactions between nearest neighbours vanish. With this assumption, a Dzyaloshinsky–Moriya interaction exists only on the J' bonds and the D vector is perpendicular to the plane. The Hamiltonian for the Dzyaloshinsky–Moriya interaction term is given by

$$\mathcal{H}_{\mathrm{DM}} = \sum_{\mathrm{nnn}} D(s_i^x s_j^y - s_i^y s_j^x). \tag{20}$$

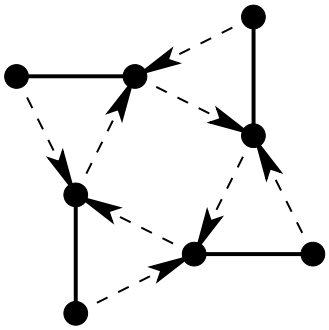

Figure 16. The unit cell for $SrCu_2(BO_3)_2$. The arrows define the directions from i site to j site for the Dzyaloshinsky–Moriya interactions in Hamiltonian (20).

For this interaction it is necessary to define the direction from i to j for a pair i, j, which is shown in figure 16.

Strictly speaking, in the real material at low temperatures (<395 K) the mirror symmetry concerning the ab plane is lost [34]. As described in section 2.1, there is a buckling in the plane. In this way, the other components of the Dzyaloshinsky–Moriya interaction exist. However, the magnitude of the buckling is small and therefore these components might be neglected, or at least expected to be smaller than those given by equation (20).

Following the argument by Cépas *et al* [65], let us start from the perturbation calculation in the limit $D/J \ll 1$ and $J' = 0$, to see the effect of the Dzyaloshinsky–Moriya interaction. In contrast to the case of next-nearest-neighbour interaction J', the triplet excitation with $S^z = \pm 1$ can hop from the first-order of the perturbation. In the orthogonal dimer model, there are two nonequivalent dimers, i.e. horizontal and perpendicular ones. The unit cell contains one horizontal dimer and one vertical dimer. For a triplet excitation, the excitation may sit either on the horizontal bond or the vertical bond. When $S^z = \pm 1$, there are matrix elements of the Dzyaloshinsky–Moriya interaction between the two states. Using a Fourier transformation, a 2×2 matrix is obtained,

$$\begin{pmatrix} J & \mp 2\mathrm{i}Df(\boldsymbol{q}) \\ \pm 2\mathrm{i}Df(\boldsymbol{q}) & J \end{pmatrix}, \tag{21}$$

where $f(\boldsymbol{q}) = \cos(q_x a/2)\cos(q_y a/2)$. The dispersion of the two modes is written as $\omega_q^{\pm} = J \pm 2D\cos(q_x a/2)\cos(q_y a/2)$. On the other hand, the Dzyaloshinsky–Moriya interaction has no effect on the $S^z = 0$ component of the triplet, so that its energy remains equal to J. We notice that the effects of J' up to fifth-order can be easily included in the above matrix in the case $D/J \ll J'/J < 1$ by replacing J in the matrix (21) by the spin gap Δ, because of the localized nature of the triplet. In that sense, the effects of J'/J up to fifth-order do not change the dispersion relations and so the results of the first-order perturbation of D might be a good approximation even for relatively large J'/J through the renormalization of J by Δ. This fact is consistent with the results of numerical calculations on finite systems [65].

At $\boldsymbol{q} = 0$, there are two upper modes with $S^z = \pm 1$, two lower modes $S^z = \pm 1$ and two $S^z = 0$ modes. A magnetic field parallel to the c-axis, $H_{\parallel}$, splits the former two modes into four branches. As shown in figure 17(a), this is consistent with the results of ESR and inelastic neutron scattering experiments. The Dzyaloshinsky–Moriya interaction also produces a splitting in a transverse magnetic field $H_{\perp}$. Including the magnetic field $H_{\perp}$, the dispersions of the modes are rewritten as $\omega_q^{\pm} = J \pm \sqrt{4D^2 f(\boldsymbol{q})^2 + (g_{\perp}\mu_B H_{\perp})^2}$, $\omega_q^0 = J$. These forms also describe the ESR results well [65] and are consistent with results of exact

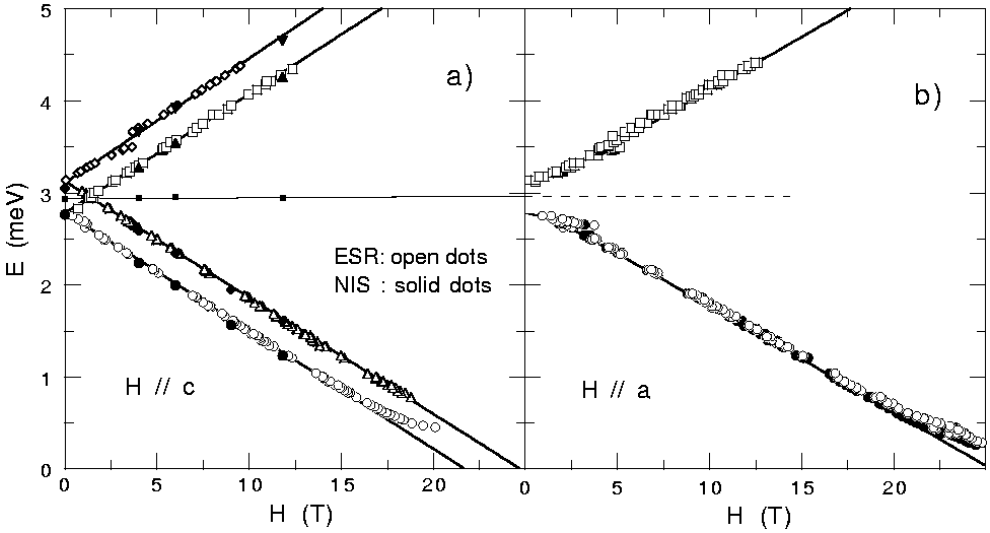

Figure 17. The magnetic field dependence of the triplet energies: (a) $H \| c$ and (b) $H \| a$ (reproduced from [65]).

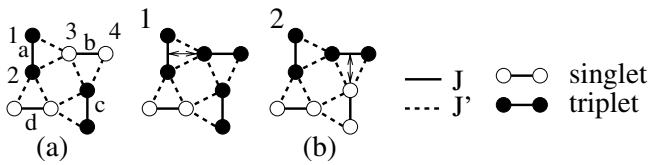

Figure 18. One of the processes of the correlated hopping. The triplet excitation on bond c can hop to bond b in the second-order perturbation (reproduced from [73]).

diagonalizations [66]. From the splitting of the first excited state at $\boldsymbol{q} = 0$, the magnitude of the Dzyaloshinsky–Moriya interaction is estimated to be $D = 2.1$ K (0.18 meV) [65] or $D = 1.7$ K (0.15 meV) [66].

4.2. Bound states of two triplets

In some of the low-dimensional spin systems of $CuGeO_3$ and NaV_2O_5, bound states of two elementary triplets have been observed [67, 68]. Also in $SrCu_2(BO_3)_2$ several excitations considered to be bound states of two triplets were observed in various experiments, as shown in table 3. In inelastic neutron scattering experiments in particular these excitations show a dispersive character contrary to the almost localized excitations observed for the lowest branch [24]. This dispersive character can be well explained as being due to the bound states of two-triplet excitations [58, 63, 69].

To illustrate the mechanism of bound states in the orthogonal dimer model, the effective bosonic representation $\boldsymbol{t}^\dagger$ in terms of triplet excitations on the J bond may be useful [32, 63]. Here $\boldsymbol{t}$ is defined as

$$t_x^\dagger|s\rangle = -\frac{1}{\sqrt{2}}(|\uparrow\uparrow\rangle - |\downarrow\downarrow\rangle), \tag{22}$$

Table 3. Excited state energies above the spin gap Δ which are observed by various experiments.

Method	Excited energies (K)					
ESR [70]	54.7, 56.2, 57.1, 58.8	64.8				
Neutron scattering [24]	58			113		
Raman scattering [32]	43		66	81	101	
Far infrared [33]	54		62	75	99	121

$$t_y^\dagger|s\rangle = \frac{\mathrm{i}}{\sqrt{2}}(|\uparrow\uparrow\rangle + |\downarrow\downarrow\rangle), \tag{23}$$

$$t_z^\dagger|s\rangle = \frac{1}{\sqrt{2}}(|\uparrow\downarrow\rangle + |\downarrow\uparrow\rangle), \tag{24}$$

where $|s\rangle$ is the singlet state. The effective Hamiltonian is written as

$$\mathcal{H} = \sum_{\alpha=A,B} J\left(-\frac{3}{4} + \boldsymbol{t}_\alpha^\dagger \boldsymbol{t}_\alpha\right) + \sum_{(\alpha,\beta)=\langle A,B\rangle} \frac{J'}{2}[(\boldsymbol{e}_\alpha \times \boldsymbol{e}_\beta)_z\{\mathrm{i}\boldsymbol{t}_\alpha^\dagger \cdot (\boldsymbol{t}_\beta \times \boldsymbol{t}_\alpha) + (\text{h.c.})\} + \boldsymbol{T}_\alpha \cdot \boldsymbol{T}_\beta] \tag{25}$$

where $\boldsymbol{T}_\alpha$ denotes the $S = 1$ operators. A unique geometrical property of the orthogonal dimer model allows nontrivial two-particle hopping called correlated hopping [71, 72], which comes from the term $\boldsymbol{t}_\alpha^\dagger \cdot (\boldsymbol{t}_\beta \times \boldsymbol{t}_\alpha)$, but neither one-particle hopping ($\boldsymbol{t}_{\alpha+x}^\dagger \boldsymbol{t}_\alpha$) nor pair creation and annihilation of triplets. Unit vectors $\boldsymbol{e}_A$ and $\boldsymbol{e}_B$ are introduced to determine the sign of the term $\boldsymbol{t}_\alpha^\dagger \cdot (\boldsymbol{t}_\beta \times \boldsymbol{t}_\alpha)$ and are defined by $\boldsymbol{e}_A = (1, 0, 0)$ and $\boldsymbol{e}_B = (0, 1, 0)$. For the motion of two triplets, matrix elements occur from the second order of the perturbation $(J'/J)^2$. One example of such a process is shown in figure 18.

In the orthogonal dimer model, the lowest branch of excited states has an almost localized nature, as emphasized before. Therefore the correlated hopping may play an important role in contrast to the usual cases. Several works about bound states have been published to explain the excitations observed in various experiments (table 3) [58, 63, 69]. We review the properties of the bound states following the argument presented in [63], using the effective Hamiltonian calculated by the perturbation [63]. However, we will skip details of the other types of method (perturbation expansion [69] and the perturbative unitary transformation by flow equations [58]) and only show their important results.

Collecting all two-particle processes up to $(J'/J)^3$, an equation for the two-particle coherent motion is closed within the four states shown in figure 19. Two of them $b(\boldsymbol{r})$ and $c(\boldsymbol{r})$ are states where two triplets exist on nearest-neighbour bonds and the others $a(\boldsymbol{r})$ and $d(\boldsymbol{r})$ are those on next-nearest-neighbour bonds. These four states are decoupled from other states where two triplets are far apart. We can introduce the pair excited states as

$$\sum \exp(\mathrm{i}\boldsymbol{P} \cdot \boldsymbol{r}_i)\{c_1(\boldsymbol{P})a(\boldsymbol{r}_i) + c_2(\boldsymbol{P})b(\boldsymbol{r}_i) + c_3(\boldsymbol{P})c(\boldsymbol{r}_i) + c_4(\boldsymbol{P})d(\boldsymbol{r}_i)\}. \tag{26}$$

Their energy spectra are calculated by diagonalizing the following 4×4 hopping matrix:

$$\begin{pmatrix} 2\Delta + V_{\mathrm{NNN}} & J_{\mathrm{NN}} & J_{\mathrm{NN}}\mathrm{e}^{\mathrm{i}p_y} & 0 \\ J_{\mathrm{NN}} & 2\Delta + V_{\mathrm{NN}} & J_{\mathrm{3rd}} & -J_{\mathrm{NN}}\mathrm{e}^{-\mathrm{i}p_x} \\ J_{\mathrm{NN}}\mathrm{e}^{-\mathrm{i}p_y} & J_{\mathrm{3rd}} & 2\Delta + V_{\mathrm{NN}} & -J_{\mathrm{NN}} \\ 0 & -J_{\mathrm{NN}}\mathrm{e}^{\mathrm{i}p_x} & -J_{\mathrm{NN}} & 2\Delta + V_{\mathrm{NNN}} \end{pmatrix} \tag{27}$$

where

$$
\begin{aligned}
V_{\mathrm{NN}} &= \left(\frac{1}{2}J' - \frac{(J')^2}{4J} - \frac{(J')^3}{2J^2}\right)\boldsymbol{T}_1\cdot\boldsymbol{T}_2 - \left(\frac{(J')^2}{4J} + \frac{(J')^3}{8J^2}\right)(\boldsymbol{T}_1\cdot\boldsymbol{T}_2)^2 + \left(\frac{(J')^2}{J} + \frac{(J')^3}{2J^2}\right) \\
V_{\mathrm{NNN}} &= \frac{(J')^3}{4J^2}\boldsymbol{T}_1\cdot\boldsymbol{T}_2 \\
J_{\mathrm{NN}} &= \left(\frac{(J')^2}{4J} + \frac{(J')^3}{4J^2}\right)\boldsymbol{T}_1\cdot\boldsymbol{T}_2 + \frac{(J')^3}{16J^2}(\boldsymbol{T}_1\cdot\boldsymbol{T}_2)^2 \\
J_{\mathrm{3rd}} &= \frac{(J')^3}{8J^2}\boldsymbol{T}_1\cdot\boldsymbol{T}_2 - \frac{(J')^2}{4J}(\boldsymbol{T}_1\cdot\boldsymbol{T}_2)^2 + \left(\frac{(J')^2}{2J} + \frac{(J')^3}{4J^2}\right).
\end{aligned}
\tag{28}
$$

The operators $\boldsymbol{T}_{1,2}$ denote a spin-1 operator. Δ is the spin gap energy and the meaning of the interactions V_{NN} and V_{NNN} and the hopping amplitudes J_{NN} and J_{3rd} can be read off from figure 19. Once we have derived the third-order effective Hamiltonian (27), no further approximation is necessary for the two-triplet motion. Diagonalizing the matrix (27), we obtain eight branches for each total spin and some of them are stable below the two-particle threshold. As expected from the analysis of the correlated hopping, the dispersion of the bound state is relatively large compared with that of the single-triplet excitations. For example, the dispersion curves with total spin $S = 1$ for $J'/J = 0.2$ and 0.5 are shown in figure 20. (The results for other total spins are shown in [63].) The minimum energy at $(0, 0)$ for $J'/J \leqslant 0.425$ is given by

$$E_{S1}/J = 2\Delta - J_{\mathrm{3rd}} + V_{\mathrm{NN}}, \tag{29}$$

and for $J'/J \geqslant 0.425$

$$
\begin{aligned}
E_{S1}/J = 2\Delta &+ \tfrac{1}{2}J_{\mathrm{3rd}} + \tfrac{1}{2}V_{\mathrm{NN}} + \tfrac{1}{2}V_{\mathrm{NNN}} - \tfrac{1}{2}(16J_{\mathrm{NN}}^2 + J_{\mathrm{3rd}}^2 + 2J_{\mathrm{3rd}}V_{\mathrm{NN}} \\
&+ V_{\mathrm{NN}}^2 - 2J_{\mathrm{3rd}}V_{\mathrm{NNN}} - 2V_{\mathrm{NN}}V_{\mathrm{NNN}} + V_{\mathrm{NNN}}^2)^{1/2}.
\end{aligned}
\tag{30}
$$

Branches calculated by Fukumoto and Knetter *et al* [58, 69] are also shown in figure 20(b). They construct the effective Hamiltonian (27) up to fifth order and after that solve the matrix by using perturbation calculation. For small J'/J, for example $J'/J = 0.2$, their results are consistent with those calculated by Totsuka *et al* [63]. However, for large J'/J, for example $J'/J = 0.5$, neither result is consistent with the other quantitatively. Thus, in both methods, it is possible to describe the magnetic behaviours of the bound states qualitatively but it is difficult to describe them quantitatively.

At the particular points $(0, 0)$ and (π, π), Knetter *et al* [58] calculated the energies up to 14th order, based on the perturbative unitary transformation by flow equations. They claim that the lowest mode at $(0, 0)$ for $S = 1$ shows an instability at $J'/J = 0.63$. On the other hand, the bound state $S = 0$ is stable for $J'/J < 0.7$. This is unusual since the binding energy is expected to be largest for $S = 0$. We consider that such an instability occurs because of an artefact of their method. In fact, such an instability has not been observed in the numerical exact diagonalization studies for up to 24 sites.

Finally, we mention the bound state with $S = 2$. The bound state with $S = 2$ can be stable because of the energy gain from the correlated hopping, although there are repulsive interactions between two-triplet excitations [72]. This fact indicates that the nonplateau state at low magnetization might be represented by a superfluid of bound states because $S = 2$ bound states have lower energy than twice the spin gap energy in the third-order perturbation calculations. However, at present the features of the nonplateau state are not yet clear and further investigations are needed.

As shown in table 3, the bound states are observed in several experimental methods. But not all of the bound states are observable because of the selection rules, which originate from

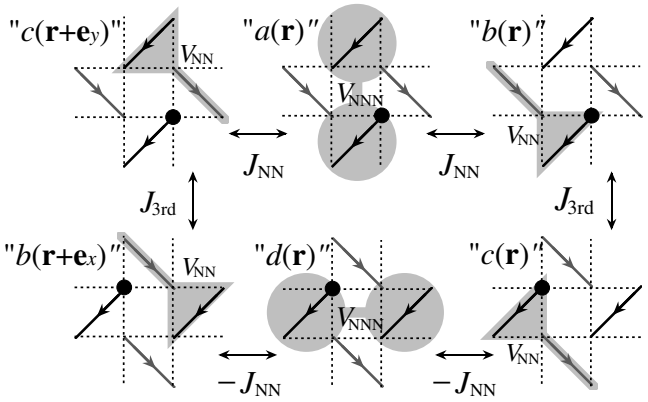

Figure 19. Hopping processes of two-triplet excitations and interactions between them. A (B) dimers are shown by bold black (gray) lines. (reproduced from [63]).

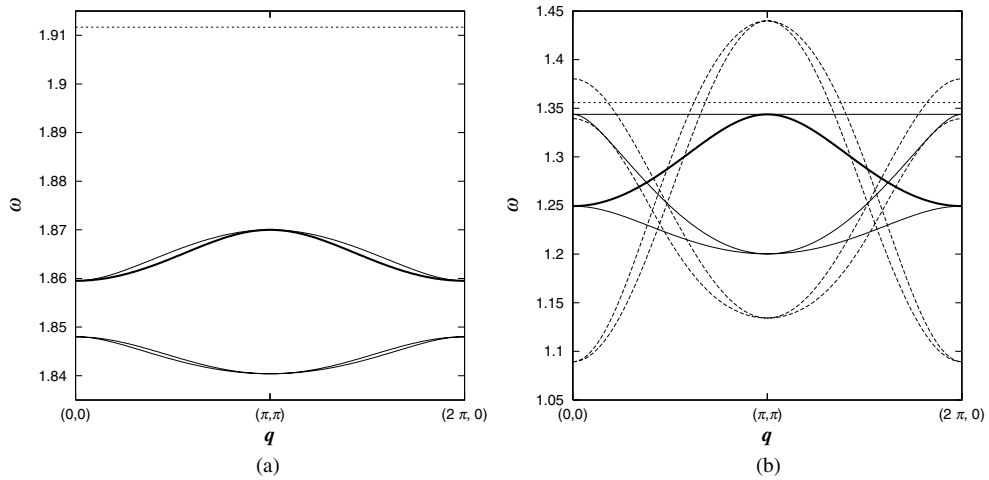

Figure 20. Triplet ($S = 1$) dispersion in the [1, 1, 0]- for (a) $J'/J = 0.2$ and (b) $J'/J = 0.5$. Curves are the results in [63]. The branches shown by the solid curves are observable in the inelastic neutron scattering experiment. Dashed curves in figure (b) are those in [58, 69]. For $J'/J = 0.2$, both results are consistent. It is difficult to distinguish two results and so only the results in [63] are shown. Twice of the spin gap lies at (a) 1.912 J and (b) 1.356 J (dotted straight lines).

the unique structure of the orthogonal dimer model. Let us consider the selection rules for a Raman scattering experiment [32, 58] and an inelastic neutron scattering experiment [63]. Finally we will comment on the selection rule for ESR [31, 65].

(1) Raman scattering experiment. In a spin system, the Raman operator obtained in second-order perturbation theory with virtual states containing one doubly occupied site is written as

$$H_R = \sum_{ij} (\boldsymbol{E}_{in} \cdot \boldsymbol{r}_{i,j})(\boldsymbol{E}_{out} \cdot \boldsymbol{r}_{i,j}) \boldsymbol{s}_i \cdot \boldsymbol{s}_j, \tag{31}$$

where $\boldsymbol{E}_{in}$ and $\boldsymbol{E}_{out}$ are the polarization vectors of incoming and scattered light and $\boldsymbol{r}_{i,j}$ is the unit vector connecting the sites i and j [74, 75]. For simplicity, the sum is taken over nearest-

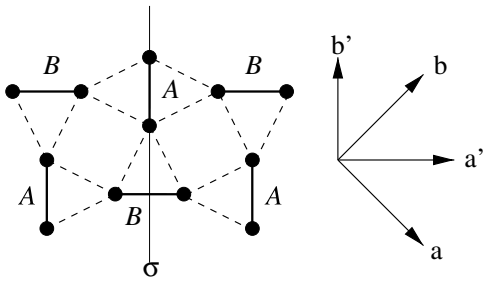

Figure 21. The orthogonal dimer model for $SrCu_2(BO_3)_2$. Two types of polarization $(\boldsymbol{ab})$ and $(\boldsymbol{a}'\boldsymbol{b}')$ are shown by arrows. The reflection axis σ is shown by a thin line.

neighbour and next-nearest-neighbour bonds. The scattering intensity is given by Fermi's golden rule

$$I(\omega) = \sum_n |\langle n|H_R|\Phi\rangle|^2 \delta(\omega - (E_n - E_0)), \tag{32}$$

where $|\Phi\rangle$ is the ground state, $|n\rangle$ are the excited states and E_0 and E_n are their energies. Thus the excitations $|n\rangle$ which satisfy the condition $\langle n|H_R|\Phi\rangle \neq 0$ can be observed in a Raman scattering experiment.

Let us consider two types of polarization $(\boldsymbol{ab})$ and $(\boldsymbol{a}'\boldsymbol{b}')$ (shown in figure 21). First of all, the Raman operator for nearest-neighbour terms does not create excitations from the ground state for any polarization, since the ground state is an eigenstate of $\sum_{\langle nn\rangle} \boldsymbol{s}_i \cdot \boldsymbol{s}_j$. On the other hand, through the Raman operator for next-nearest-neighbours, the polarization $(\boldsymbol{a}'\boldsymbol{b}')$ can create excitations from the ground state but the $(\boldsymbol{ab})$ polarization cannot, as pointed out by Knetter *et al* [58]. These facts originate from the parity of the Hamiltonian. Let us consider the simplest case as in figure 6(b). In the $(\boldsymbol{a}'\boldsymbol{b}')$ polarization the Raman operator has odd parity to the reflection of the lattice, on the other hand in the $(\boldsymbol{ab})$ polarization it has even parity. The singlet on a bond has odd parity. By symmetry, only the antisymmetric part of H_R can create excitations from the ground state. In fact, in Raman experiments a relatively big peak is observed around 3.0 meV for the polarization $(\boldsymbol{a}'\boldsymbol{b}')$, which corresponds to the bound state with $S = 0$, but for $(\boldsymbol{ab})$ the intensities almost vanish [32].

From the above simple discussion, it is expected that there should be no intensity for the polarization $(\boldsymbol{ab})$. However, there is still a finite intensity in the experiment. In addition to this, the spin gap, i.e. the transition $\Delta S = 1$, is also observed in Raman experiments. The Raman operator (31) allows transitions with $\Delta S = 0$. These facts indicate that a mechanism beyond the Raman operator (31) should be needed. One possible way to understand these phenomena might be the inclusion of the Dzyaloshinsky–Moriya interaction. However, it is still an open question whether this is sufficient or not.

(2) Inelastic neutron scattering experiment. In the inelastic neutron scattering experiment, excited states with $S = 1$ are generally observed. However, only several branches of the bound states with $S = 1$ are observed because of the unique structure of $SrCu_2(BO_3)_2$. The Fourier transform $S^j(\boldsymbol{q})$ of local spin operators creates single-triplet states

$$S^j(\boldsymbol{q})|\Psi\rangle = f_q^+ t_{A,j}^\dagger |\Psi\rangle + f_q^- \mathrm{e}^{-\mathrm{i}(l/2)(q_x+q_y)} t_{B,j}^\dagger |\Psi\rangle \tag{33}$$

over the dimer singlet ground state, where $|\Psi\rangle$ is the ground state (5). On the symmetry lines $q_x = \pm q_y$, one of the structure factors $f_\pm = \mp \mathrm{i} \sin[l(q_x \pm q_y)/2\sqrt{2}]$ vanishes and thus, only an A(B) triplet is excited. Although only a single triplet is contained in the state (33),

the perturbation broadens the wavefunction and $S^j(\boldsymbol{q})|\Psi\rangle$ can have a finite overlap with two-triplet states. Since $S^j(q_x, \pm q_y)|\Psi\rangle$ is even under the reflection σ shown in figure 21, any state which is connected to $S^j(\boldsymbol{q})|\Psi\rangle$ by perturbation should be also even; any bound state whose wavefunction contains 'b' and 'c' in an antisymmetric manner is orthogonal to $S^j(\boldsymbol{q})|\Psi\rangle$. Therefore inelastic neutron experiments along the [110]([1$\bar{1}$0]) direction detect only bound states shown by solid lines in figure 20. Qualitative features agree well with the dispersion observed in the experiment [24].

To compare with experimental results quantitatively, the dynamical structure factor $S(q, \omega)$ was calculated by using exact diagonalizations [73]. The dynamical structure factor $S(q, \omega)$ at $T = 0$ is defined by

$$S(\boldsymbol{q}, \omega) = \sum_n |\langle n|S^z(\boldsymbol{q})|\Psi\rangle|^2 \delta(\omega - E_n + E_0), \tag{34}$$

where $|n\rangle$ are the excited states, E_n their energies and E_0 is the ground state energy. The spin density operator $S^z(\boldsymbol{q})$ is defined by $S^z(\boldsymbol{q}) = \frac{1}{\sqrt{N}} \sum_i \mathrm{e}^{\mathrm{i}\boldsymbol{q}\cdot\boldsymbol{r}_i} S_i^z$. $S(\boldsymbol{q}, \omega)$, which is explicitly expressed in terms of the continued fraction

$$S(q, \omega) = -\frac{1}{\pi} \mathrm{Im} \frac{\langle\Psi|S_q^{z\dagger} S_q^z|\Psi\rangle}{z - a_0 - \frac{b_1^2}{z - a_1 - \cdots}}, \tag{35}$$

can be calculated directly by the Lanczos method. Here $z = \omega + E_0 + \mathrm{i}\epsilon$. For the fit we use $\epsilon = 0.1$ as the damping constant. The results for $N = 24$ at $\boldsymbol{q} = (2\pi, 2\pi)$ with $J = 85$ K and $J' = 54$ K are shown in figure 22. The result agrees well with the experimental results. As a reference, the results for $N = 20$ and 24 with $\epsilon = 0.01$ are also shown. The first big peak at 3 meV (35 K) is due to the spin gap excitation. It hardly depends on the system size because of its localized nature. The second peak exists around 60 K. It corresponds to the excitation which is observed around 5 meV (58 K) in the experiment. We conclude that the main contribution to this excitation is due to the bound states of two triplets. The bound states have a dispersive character as shown in figure 15 and this is indeed revealed in the inelastic neutron scattering experiment as a considerable width of the second peak.

Finally we comment on the excitations around 9 meV (104 K). They consist of many peaks and their origin is not yet clear [24]. We only mention that there are three possibilities: (i) (anti) bound states of two triplets, (ii) continuum of two or more triplets and (iii) bound states of three triplets.

Recently, a neutron scattering experiment with high resolution (the same resolution as in [65]) was done for the bound states [76]. The experimental results are consistent with those of ESR [70] and several excited states are observable. The origin of each peak is not yet clear and the effect of the Dzyaloshinsky–Moriya interaction might be important in explaining some of these results like the splitting of the lowest branch of the excitations.

(3) ESR. ESR is an important experimental method to investigate magnetic excitations. In particular it is useful for studying the external magnetic field dependence of the magnetic excitations, since it is possible to measure an ESR signal in high magnetic fields. The critical field for $SrCu_2(BO_3)_2$ is above 20 T and thus methods for measuring magnetic excitations in such high fields are limited. Nojiri *et al* [31, 70, 77, 78] observed magnetic excitations using ESR up to 55 T and found many excitations. However, the theory of ESR in quantum spin systems is not fully developed yet, especially in the case where quantum fluctuations are important [79]. Further theoretical developments are necessary to analyse the results of ESR completely. Here we briefly describe several possible scenarios.

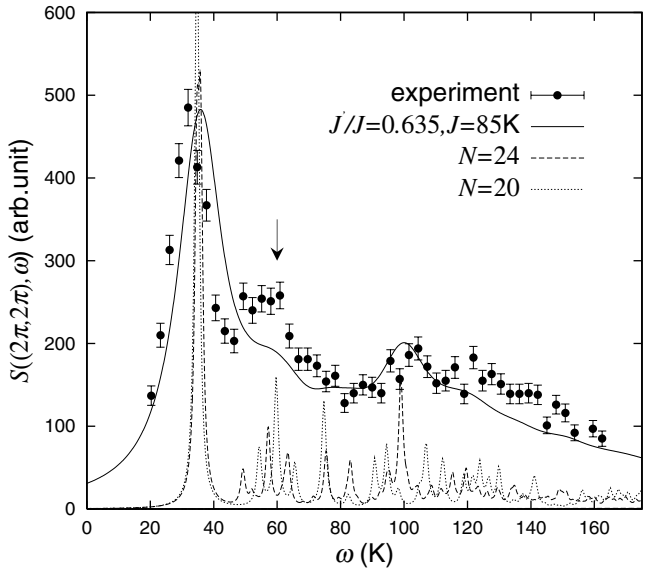

Figure 22. Theoretical result of $S((2\pi, 2\pi), \omega)$ is compared with the experimental results. The results for $N = 20$ and 24 with $\epsilon = 0.01$ are also shown (reproduced from [73]).

In principle, ESR can observe the transitions satisfying the condition $\Delta S = 0$ and $\Delta S^z = \pm 1$ in spin systems. However, in $SrCu_2(BO_3)_2$ transitions from the singlet ground state to the excited triplet states were observed [31]. As indicated by Nojiri *et al*, some mechanism which breaks the rotational symmetry of the spin space like Dzyaloshinsky–Moriya interaction, nonequivalent g-tensors or anisotropic exchange interaction is necessary to make the transition observable.

However, Cépas *et al* [65] pointed out that the Dzyaloshinsky–Moriya interaction or anisotropic exchange interaction alone cannot explain the transition because of symmetry. Also they mentioned that with the anisotropy of the g-tensors or with both the Dzyaloshinsky–Moriya interaction and an anisotropic exchange interaction the transition is possible in principle but should be very small. They proposed electric dipole transition by a phonon assisted mechanism to be the origin of the observed transition. They calculated the effective operator H_{ESR} treating the spin–phonon interaction λ perturbatively in a purely electronic mechanism. The effective operator is written as $H_{ESR} = \sum_{\mathrm{nn}} \gamma \boldsymbol{s}_i \cdot \boldsymbol{s}_j + \eta \cdot (\boldsymbol{s}_i \times \boldsymbol{s}_j)$: the first term is a transition via a virtual phonon as an intermediate state and the second occurs from a spin–orbit coupling λ. Here $|\eta| \sim \lambda\gamma$. This effective operator gives an intensity proportional to η^2, which might be consistent with the experiment results.

At this stage, electric dipole transition is suggested as the possible origin of the ESR transition. However, the mechanism of the transition is not yet clear and further investigation is needed.

5. Estimation of the coupling constants for $SrCu_2(BO_3)_2$—thermodynamic properties

In this section, we will discuss an optimal set of coupling constants for $SrCu_2(BO_3)_2$ by fitting various thermodynamic properties.

As shown in section 4.1, the lowest triplet excitations have an almost flat band. Therefore it is difficult to determine both J and J' only from the dispersion relation of the lowest excited

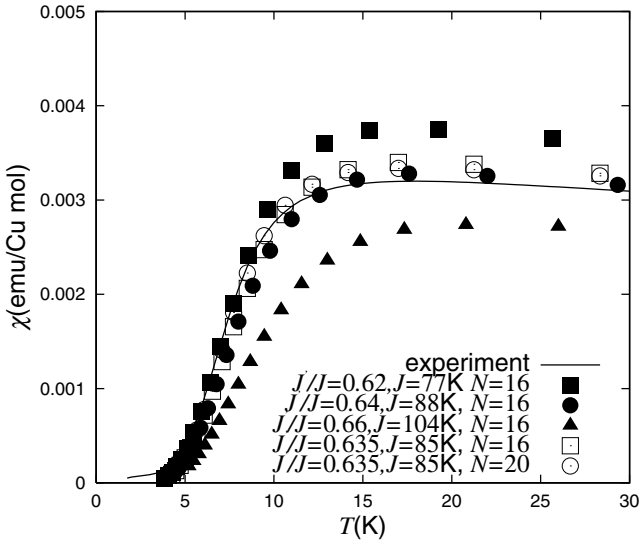

Figure 23. The temperature dependence of the magnetic susceptibility $T < 30$ K. The results with the parameters $J = 72$ K for $J'/J = 0.62$, $J = 88$ K for $J'/J = 0.64$, and $J = 104$ K for $J'/J = 0.66$ are shown by the full symbols. The results with the optimal set $J'/J = 0.635$ and $J = 85$ K are shown by the open symbols (reproduced from [60]).

states observed in inelastic neutron scattering experiments, in contrast to usual spin systems. One of the possible ways to estimate the parameters is to fit the temperature dependence of the magnetic susceptibility [60]. For a given ratio of J'/J, the value of J is determined so that the spin gap obtained from the exact diagonalization is 35 K. For the estimation of the spin gap, a system with $N = 24$ spins is sufficient. Temperature dependence of the susceptibility is calculated by using the transfer matrix method for finite clusters. In figure 23, calculated results of $\chi_{2d}(J'/J)$ for the system with $N = 16$ spins are compared with experimental results for various $J'/J = 0.62, 0.635, 0.64, 0.66$. The best fit is obtained for $J'/J = 0.635$ and $J = 85$ K. It should be noted that the series expansion up to 25th order [54] gives a spin gap of 34.3 K, which is consistent with the observed spin gap. To check the finite size effect for this set of parameters, the result for $N = 20$ is also shown in figure 23. In the present system, the finite size effect is not so important since the lowest branch of the triplet excitations is almost localized.

However, the temperature dependence of the calculated susceptibility for this set of parameters does not fit the experimental results well at $T > \Delta$. This fact suggests that the effects of the interlayer coupling J'' (figure 7) on the susceptibility cannot be neglected in such a high temperature range as discussed in section 4.1. To see the effects of the interlayer coupling, we assume the mean-field type scaling ansatz used in [80]:

$$\chi(J'/J, J''/J) = \frac{\chi_{2d}(J'/J)}{1 + 4J''\chi_{2d}(J'/J)}. \tag{36}$$

The coefficient $4J''$ in the denominator reproduces correctly the high-temperature Weiss constant of the three-dimensional model. At low temperatures this ansatz gives the same spin gap as that given by the two-dimensional model, which is reasonable because the spin gap is not modified by J''. From the fitting at $T > \Delta$, $J''/J = 0.09$ is obtained as the best choice. The result of the fitting is shown in figure 2.

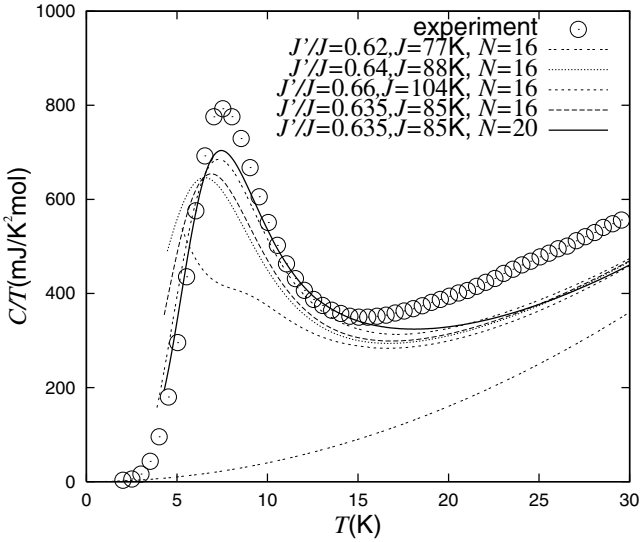

Figure 24. The temperature dependence of the specific heat $T < 30$ K.The results with the parameters $J = 72$ K for $J'/J = 0.62$, $J = 88$ K for $J'/J = 0.64$, and $J = 104$ K for $J'/J = 0.66$ are shown by the thin curves. The results with the optimal set $J'/J = 0.635$ and $J = 85$ K are shown by the solid curve (reproduced from [60]).

Strictly speaking, two different types of interlayer interaction J_1'' and J_2'' are necessary at $T < 395$ K because of the buckling of the $CuBO_3$ plane (see figure 5(a)). In the mean-field type approximation, J''/J estimated in this way gives the average value of the interlayer couplings. It is difficult to estimate the coupling constants beyond the mean field level.

These parameters $J = 85$ K and $J' = 54$ K can also reproduce the temperature dependence of the specific heat of $SrCu_2(BO_3)_2$ at low temperatures $T < 15$ K [30, 81] as shown in figure 24 [60] and the excitations observed by inelastic neutron scattering as shown in figure 15 and 22 [63, 73]. In figure 24, the phonon term $\beta \times T^3$, where $\beta = 0.4$ mJ K^{-4}, has been assumed. At temperatures $T > 15$ K, a good quality of the fits is not obtained. Possible reasons for this difference may be the following: (i) the simple $\beta \times T^3$ expression is not sufficient for the lattice contribution; (ii) the effects of the spin–phonon coupling are important. In the orthogonal dimer model, the small kinetic energies of the excited triplets originate from the geometrical constraint. When the orthogonality is broken by some distortion of dimer bonds, a finite matrix element for the hopping of a triplet arises. Therefore a triplet excitation is expected to be strongly coupled with phonons.

Finally, we comment on various choices of coupling constants. Initially, and then frequently, $J'/J = 0.68$ and $J = 100$ K were used as the optimal values for $SrCu_2(BO_3)_2$ [35]. However, these parameters are estimated from the experimental results of the powder sample with the spin gap 30 K, which is smaller than the intrinsic value of 35 K. Another set $J'/J = 0.603$, $J''/J = 0.21$ and $J = 71$ K (6.16 meV) was proposed by Knetter *et al* [58] from the bound state energies of the two-triplet excitations. This set of parameters, however, does not reproduce the temperature dependence of the magnetic susceptibility at $T < \Delta$ as shown in figure 23. Thus we conclude that the parameter $J'/J = 0.635$ is the optimal set for this material, better than $J'/J = 0.68$ and 0.603.

6. Magnetization

One of the most remarkable experiments on $SrCu_2(BO_3)_2$ is the observation of magnetization plateaux at 1/8, 1/4 and 1/3 of the full Cu^{2+} moment (figure 3) [22, 25, 26].

The triplet excitations in this system have a very small kinetic energy, as already stressed. Applying an external magnetic field, we change the density of triplets. In general, there is competition between the kinetic energy of the excited triplets and the repulsive interaction energy between the triplets. At certain densities, i.e. magnetizations where the commensurability energy is significant, it is natural to expect that the crystallization of the triplet excitations, leading to a finite energy gap and a magnetization plateau, is particularly favourable.

6.1. Effective hard-core boson model

The appearance of plateaux in one-dimensional models has been discussed from the view point of metal–insulator transitions of the magnetic excitations tuned by the magnetic field [15]. However, this scenario is not limited to one-dimensional systems and also applies to two- and three-dimensional systems [71, 82, 83]. The magnetization of $SrCu_2(BO_3)_2$ is also explained well in this point of view [71, 72, 84–87]. In the orthogonal dimer model, the excited triplets can be treated as particles in a sea of singlets. Under the magnetic field, it may be a good starting point to keep only two states for each nearest-neighbour bond, the singlet and the lowest triplet, as the physical degrees of freedom. By considering the triplet with $S^z = 1$ as a hard-core boson ($n_i = 1$) and the singlet as a vacancy ($n_i = 0$), the effective hard-core boson Hamiltonian is derived by the perturbation calculation from the limit $J'/J \ll 1$. The model is written as

$$\mathcal{H}_{eff} = \mathcal{H}_c + \mathcal{H}_k + \mathcal{H}_{ch} + \mathcal{H}_i = \mu \sum_i n_i + \sum_{ij} t_{ij}(c_i^\dagger c_j + \text{h.c.}) + \sum_{ijk} t_{ijk}^{ch}(c_i^\dagger c_j + \text{h.c.})n_k + \sum_{ij} V(\boldsymbol{r}_i - \boldsymbol{r}_j)n_i n_j \tag{37}$$

where $c_i^\dagger$ (c_i) creates (annihilates) a magnetic excitation at bond i, and $n_i = c_i^\dagger c_i$ is the number operator. μ is the chemical potential for bosons which is nothing but the external magnetic field, H, in the original model. In the first line, $\mathcal{H}_k$ means the hopping term and $\mathcal{H}_{ch}$ the correlated hopping term. The correlated hopping plays an important role for the bound states of two-triplet excitations as we discussed in section 4.2. $\mathcal{H}_i$ represents interactions between two triplets. The interactions up to third-order are written as

$$\frac{V_1}{J} = \frac{1}{2}\frac{J'}{J} + \frac{1}{2}\left(\frac{J'}{J}\right)^2 - \frac{1}{8}\left(\frac{J'}{J}\right)^3, \tag{38}$$

$$\frac{V_2}{J} = \frac{1}{4}\left(\frac{J'}{J}\right)^3, \tag{39}$$

$$\frac{V_3}{J} = \frac{1}{2}\left(\frac{J'}{J}\right)^2 + \frac{3}{4}\left(\frac{J'}{J}\right)^3, \tag{40}$$

$$\frac{V_3'}{J} = 0, \tag{41}$$

where V_n represents the interaction between the nth-nearest-neighbour pair of dimers (see figure 26). The interactions for $n = 3$ depend strongly on direction. For a pair of parallel dimer bonds the interaction V_3 starts from second-order corrections, while that between the

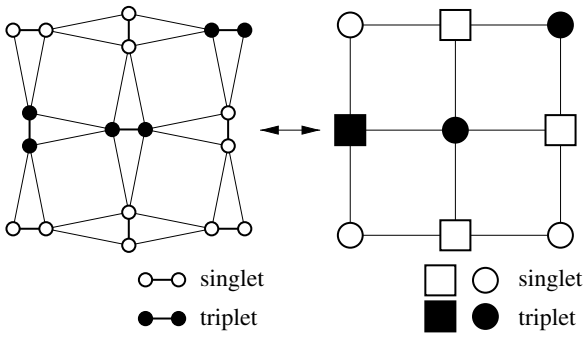

Figure 25. Mapping the orthogonal dimer Heisenberg model to a hard-core boson model on the interpenetrating two square lattices, one for vertical dimers (shown by squares) and the other for horizontal dimers (shown by circles). The singlet states are represented by open symbols and the $S^z = 1$ triplet states by full symbols.

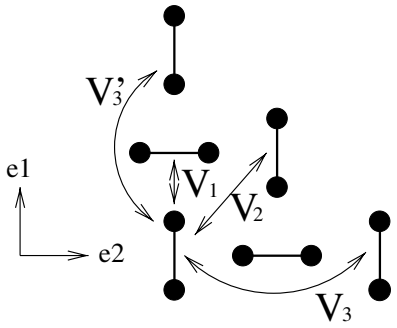

Figure 26. Interactions between the triplet excitations. The nearest-neighbour interaction V_1, the next-nearest-neighbour interaction V_2 and the third-nearest-neighbour interactions V_3 and V_3' are shown (reproduced from [84]).

dimer bonds on a straight line V_3' vanishes in low-order perturbations. In addition to that, V_3 is lager than V_2 for any J'/J. These features are characteristic of the geometry of the orthogonal dimer system. Since the kinetic energy of one particle $\mathcal{H}_k$ is much smaller than the other terms, the correlated hopping energies $\mathcal{H}_{ch}$ and the interaction energies $\mathcal{H}_i$, we may neglect this term to a first approximation.

Momoi and Totsuka [71, 72] have derived the effective Hamiltonian up to third order of J'/J. Its complete form is shown in [72]. In this order one-particle hopping terms do not appear and thus the competition is only between repulsive interactions and correlated hopping. To treat these effects, they map the hard-core boson system onto an $S = 1/2$ pseudo spin system. Then the quantum pseudo spin operators are approximated by classical vectors with fixed length. The ground state of finite size systems is obtained both by a mean-field approximation and by Monte Carlo sampling. In the latter method, the temperature is gradually decreased towards zero. In the evaluated magnetization, plateaux are observed at $m = 1/2$ and $1/3$ but not at $m = 1/4$ and $1/8$.

The classical pseudo spin configuration can be mapped onto the original $S = 1/2$ configuration (details are in [72]). The plateau states at $m = 1/2$ and $1/3$ have density-wave long-range order with checkerboard and stripe structures respectively. The results are summarized in the phase diagram of figure 27. Notice that the plateau at $1/2$ is stable only in

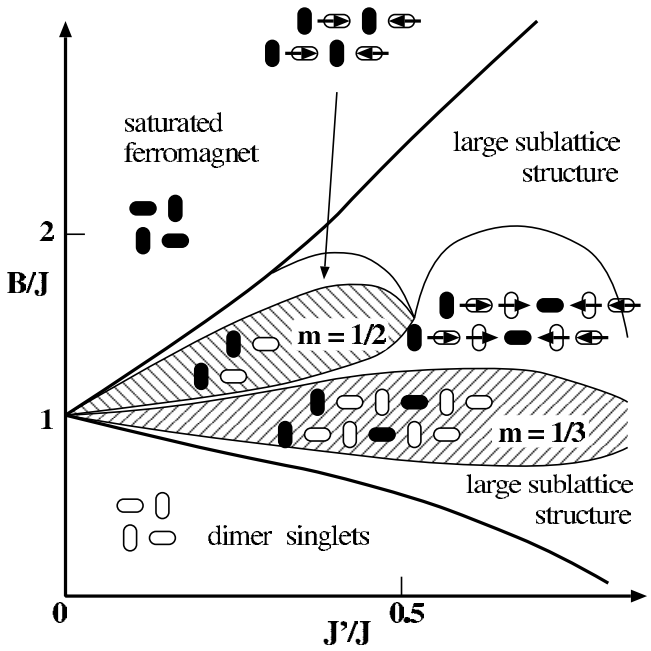

Figure 27. Phase diagram at $T = 0$ with the parameter J'/J and the magnetic field B/J (reproduced from [72]).

the region $0 < J'/J < 0.50$. For large J'/J, the correlated hopping makes the superstructure unstable; however, the phase boundary might move to larger parameters due to quantum effects in the original spin model.

In the analysis by Momoi and Totsuka, there are no plateaux at $1/4$ and $1/8$. This fact indicates that the interactions determined by the perturbation theory up to third-order are not sufficient to reproduce the $1/4$ and $1/8$ plateaux. This conclusion is supported by exact diagonalization studies in finite systems [84]. The magnetization curve for a 16-site cluster is calculated for both $J'/J = 0.4$ and 0.635. The $1/8$ plateau is obtained only for $J'/J = 0.635$ but not for $J'/J = 0.4$.

To include long-range repulsive interactions, we assume interactions with Yukawa form [84]. By the string effect discussed in section 4.1, the wavefunction of a triplet excitation is expected to have an exponential tail. Thus it is natural to assume interactions between two triplets with exponential form. As a working hypothesis we assume the following form for the interactions,

$$V(\boldsymbol{r}) = \begin{cases} V_n(V_n') & (n = 1, 2, 3) \\ V_0 \dfrac{\exp(-r/\xi)}{r} & (\text{others}). \end{cases}$$

Concerning the short-range interactions we fixed the ratios V_2/V_1 and V_3/V_1 using the perturbation results and the parameters V_0/V_1 and ξ are determined to reproduce the results of exact diagonalizations for $J'/J = 0.635$. The kinetic term and correlated hopping term are neglected: the former is small in the perturbation results and the latter may be negligible for small densities of triplet excitations. When the kinetic energies are neglected, it is straightforward to calculate the energy of every state with a fixed density of triplets, i.e. at

a certain magnetization, once the distribution of the bosons is specified,

$$\mathcal{E}_i = \sum_q V_q n_q n_{-q}, \tag{42}$$

where n_q and V_q are the Fourier components of the distribution of bosons and the interactions, respectively. We have considered periodic boundary conditions for the distributions of triplet excitations with various unit cells. For each unit cell, all possible configurations are generated and their energies are calculated. In this way, the lowest-energy states are determined for all S^z. The unit cells used are $N_d = 16, 20, 26, 32, 36$ with square unit cells and $N_d = 24, 32$ with rectangular cells. Here, N_d means the number of dimer bonds in each unit cell.

The magnetization curve thus obtained is shown in figure 28. In this calculation, the curve consists of many steps. When a kinetic energy is included small steps will be smeared out and only large steps will survive as plateaux. As possible plateaux, distinct structures of magnetization are seen at $1/2$, $1/3$, $1/4$ and $1/8$. At the same time, the classical solution for the hard-core boson model gives possible superstructures. The superstructures at these plateaux are also shown in figure 28. The structures at $1/2$ and $1/3$ are the same as those obtained by Momoi and Totsuka (figure 27). The plateau at $1/4$ is also characterized by stripe order. The $1/8$ plateau has a rhomboid unit cell. A square unit cell was also proposed for the $1/8$ plateau because of the high symmetry [35, 84]. However, recent NMR experiments indicate that a rhomboid cell is realized [28], which will be discussed in section 6.3. One may think that these structures appear because of our classical approximation. However, the spin–spin correlation functions for a finite system in the original Heisenberg model are compatible with the simple structures shown in the figure. Details of the calculation and a comparison with the classical solutions are discussed in [84].

Another approach based on the hard-core boson effective model was followed by Fukumoto and Oguchi. They carried out a partial diagonalization of the effective Hamiltonian [86, 87]. In first order of the perturbation, only the interaction V_1 exists and there is no flip part. Therefore the lowest eigenvalue of the effective Hamiltonian is zero for $0 \leqslant m \leqslant 1/2$. In this range of magnetization, the lowest-energy states have no nearest-neighbour triplet dimer pairs and therefore the states with nearest-neighbour triplet dimer pairs might be neglected. In this assumption, they partially diagonalize the third-order effective Hamiltonian within the configurations where there are no nearest-neighbour triplet dimer states and diagonalize the various finite size clusters with periodic boundary conditions: $N_D = 8$, 10, 12, and 36 where N_D is the number of dimer bonds. They observed the $1/3$ plateau, and the configuration at the plateau is a stripe state of triplets. This is consistent with the previous two results.

To study the plateaux at $m < 1/3$, Fukumoto [87] constructed the effective model up to the fourth-order perturbation in the subspace without nearest-neighbour and one type of third-neighbour (V_3) triplet pairs. Within these restricted states, the term of the next-nearest-neighbour interaction cancels the correlated hopping term in the second order of the effective model (details are in [87]). The higher-order correlated hopping terms remain. However, they neglected the effects of the correlated hopping with the hope that the energy gained due to them is small. The Hamiltonian is diagonalized for various finite-size clusters up to $N_D = 48$. The results indicate the presence of the $1/4$ plateau and its structure is a stripe state, which agrees with the result in [84]. In this effective Hamiltonian, there is a fourth-neighbour interaction V_4, which is responsible for the $1/4$ plateau.

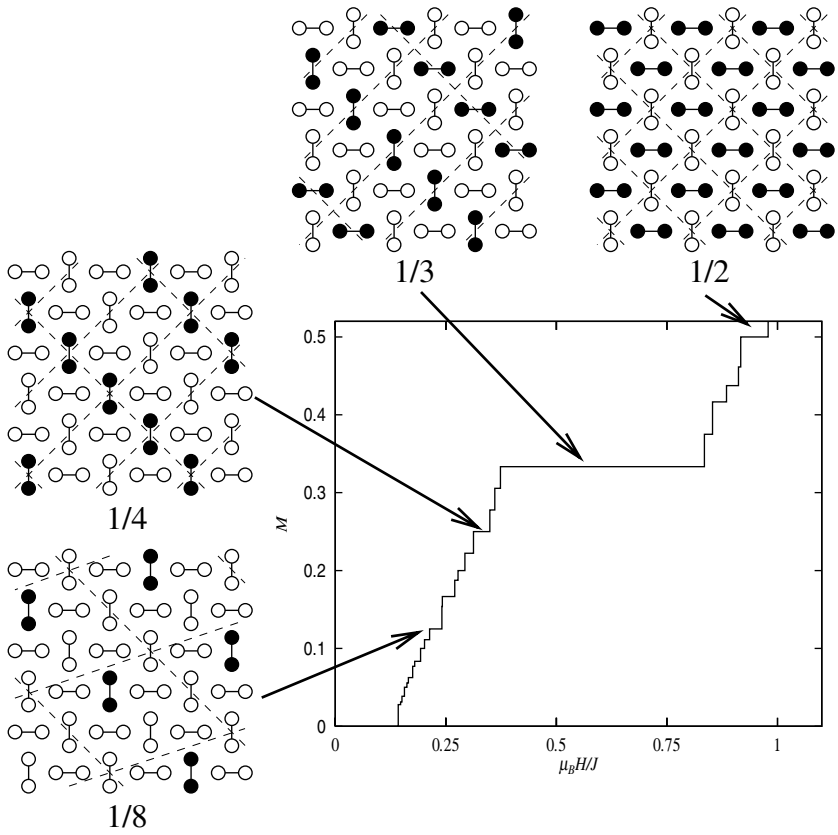

Figure 28. The magnetization curve and the structures at the plateaux. Here the triplet excitations are shown by full symbols and the singlets by the open symbols.

6.2. Chern–Simons theory

In the previous sections, the hard-core bosons, which describe the excited triplets, were used to discuss the magnetization. In this section, we follow the argument presented in [88, 89]. Let us consider the mapping from the spin operators to hard-core boson operators:

$$s_i^+ = b_i^\dagger, \tag{43}$$

$$s_i^- = b_i, \tag{44}$$

$$b_i^\dagger b_i = s_i^z + 1/2. \tag{45}$$

The original spin Hamiltonian is rewritten using the hard-core boson operators:

$$H = \tfrac{1}{2}\sum_{\rm nn} J(b_i^\dagger b_j + b_j^\dagger b_i) + \tfrac{1}{2}\sum_{\rm nn} J(n_i - 1/2)(n_j - 1/2) + \tfrac{1}{2}\sum_{\rm nnn} J'(b_i^\dagger b_j + b_j^\dagger b_i) + \tfrac{1}{2}\sum_{\rm nnn} J(n_i - 1/2)(n_j - 1/2), \tag{46}$$

where $n_i = b_i^\dagger b_i$ is the occupation number of site i. The hard-core constraint is taken into account exactly by further mapping from the hard-core bosons onto spinless fermions coupled to a Chern–Simons gauge field:

$$b_i^\dagger = s_i^+ = \mathrm{e}^{\mathrm{i}\alpha_i} f_i^\dagger, \tag{47}$$

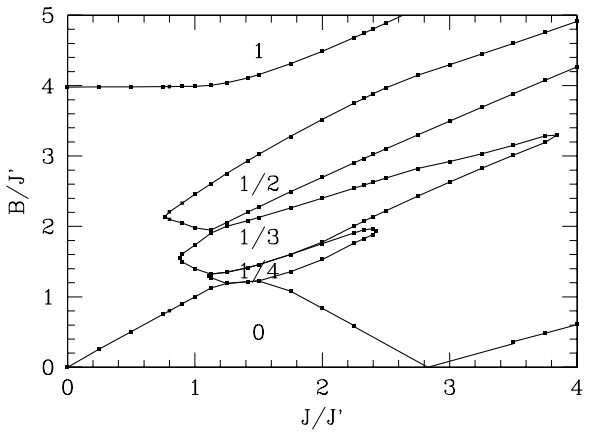

Figure 29. Phase diagram with the parameter J/J' and magnetic field B/J' (reproduced from [88]).

$$b_i = s_i^- = f_i \mathrm{e}^{-\mathrm{i}\alpha_i}. \tag{48}$$

In a mean-field approximation, the gauge field is replaced by its static mean value. The flux per square plaquette ϕ is tied to the density of fermions: the magnetization of the spin system M, since it comes from the flux tubes initially attached to each fermion

$$\frac{\phi}{2\pi} = \langle n \rangle = \left(\langle S^z \rangle + \frac{1}{2} \right) = M + \frac{1}{2}. \tag{49}$$

The Ising term in (46) takes a simple form in the mean-field decoupling and thus it becomes a simple function of the magnetization. On the other hand, the kinetic energy term in (46) leads to a Hofstadter problem. However, it is straightforward to calculate this term, since this is a one-body problem. On each triangular plaquette, flux $\phi/2$ are attached.

Equation (49) for a certain value of magnetization M defines the flux and the number of fermions. The total energy $E(M)$ is given by filling the band spectrum from the bottom with an appropriate number of fermions and adding the contribution from the Ising terms. After that, minimization $E(M) - BM$ leads to the magnetization as a function of B.

The results are summarized in figure 29 and $1/2$, $1/3$ and $1/4$ plateaux are stable. These plateaux are also observed in the effective hard-core boson models. In Chern–Simons mean-field theory, the plateau phases are still stable in the plaquette dimer singlet state $1.16 < J/J' < 1.47$ ($0.68 < J'/J < 0.86$) and the antiferromagnetic phase $J/J' < 1.16$ ($J'/J > 0.86$). In these parameter ranges, the hard-core boson models are not reliable and the present result may be considered as the first indication of the existence of plateaux in the intermediate phase. However, the spin gap in the antiferromagnetic phase may be an artefact due to the fact that the Néel state is not correctly described in the uniform mean-field approximation, as pointed out in [90]. Therefore it is necessary to compute nonuniform solutions of the mean-field Chern–Simons approach with two sublattices to conclude the existence of plateaux beyond the critical point.

Finally, it should be mentioned that Misguich *et al* [88] reproduced the qualitative shape of the experimental magnetization curve for $SrCu_2(BO_3)_2$ with $J = 71$ K and $J' = 43$ K with a good agreement between 25 and 50 T and predicted the $1/2$ plateau beginning at 60 T. But recent experiments show that the $1/3$ plateau is stable up to 70 T at least (see figure 3) [26].

6.3. Spin–lattice interactions at plateau

Calculations using the effective hard-core boson model predict a superstructure accompanied with a breaking of translational symmetry at magnetizations 1/8, 1/4 and 1/3. Recently Kodama *et al* [28] succeeded in performing NMR measurements at the 1/8 plateau. The frequency pattern of the NMR indicates that below the critical field for the 1/8 plateau the spin state is uniform. On the other hand, at the 1/8 plateau, several different spin sites have been identified. This is a direct observation of the breaking of translational symmetry. However, the very rich texture of the magnetization observed in the NMR experiments cannot be reproduced within the hard-core boson model approximation, where there are only two different spin sites. Therefore one has to go back to the original spin Hamiltonian. The presence of the 1/8 plateau is expected to lead to a breaking of the lattice symmetry and to degenerate ground states in the thermodynamic limit. One way to select a unique ground state would be to couple the system to the lattice as in the Jahn–Teller effect [91]. Actually, sound velocity experiments have revealed anomalies in the elastic constants upon entering the magnetization plateaux [92–94].

Miyahara and colleagues [28, 95] have considered the effects of adiabatic phonons. The Hamiltonian is defined by

$$\mathcal{H} = \sum_{(\mathrm{nn})} J(d_{ij})\boldsymbol{S}_i \cdot \boldsymbol{S}_j + \sum_{(\mathrm{nnn})} J'(d_{ij})\boldsymbol{S}_i \cdot \boldsymbol{S}_j + \frac{K}{2}\sum_{(\mathrm{nn})}\left(\frac{\|\delta\boldsymbol{r}_i - \delta\boldsymbol{r}_j\|}{d_{ij}^0}\right)^2 + \frac{K'}{2}\sum_{(\mathrm{nnn})}\left(\frac{\|\delta\boldsymbol{r}_i - \delta\boldsymbol{r}_j\|}{d_{ij}^0}\right)^2.$$

For small displacements of the copper atoms, it is possible to linearize the antiferromagnetic couplings around the equilibrium values:

$$J(d_{ij}) = J\left(\frac{d_{ij}^0}{d_{ij}}\right)^{\alpha} \simeq J\left[1 - \alpha\frac{\delta d_{ij}}{d_{ij}^0}\right], \tag{50}$$

$$J'(d_{ij}) = J'\left(\frac{d_{ij}^0}{d_{ij}}\right)^{\alpha'} \simeq J'\left[1 - \alpha'\frac{\delta d_{ij}}{d_{ij}^0}\right]. \tag{51}$$

The parameters α and α' are related to the derivative of the superexchange couplings with respect to the relative distance. They have studied the Hamiltonian (50) by exact diagonalization on finite clusters with the Lanczos algorithm. As mentioned in section 6.1, two possible unit cells (square and rhomboid unit cell) are proposed for the description of the 1/8 plateau in the hard-core boson model. The configuration with both unit cells has been calculated and the results for $J = 85$ K, $J' = 54$ K, $\alpha = \alpha' = 7$ and $K = K' = 20\,000$ K are sketched in figure 30. The square unit cell has six different sites, while the rhomboid has eight different sites. In both cases, the magnetization is centred around one strongly polarized dimer, with Friedel-like oscillations with alternately positive and negative magnetizations. These oscillations decay quite fast, and away from the central dimer the magnetization is very small. Therefore the finite size effects are expected to be very small and the 16-site cluster calculations to be quite a good approximation. Including the effect of the interlayer couplings, 14 sites are expected for the rhomboid cell. On the other hand, the interlayer couplings do not change the number of nonequivalent sites in the square unit cell assuming the triplet to be as far as possible in different layers. In the NMR data at least 11 different sites were identified. Therefore we expect the rhomboid cell to be realized at the 1/8 plateau.

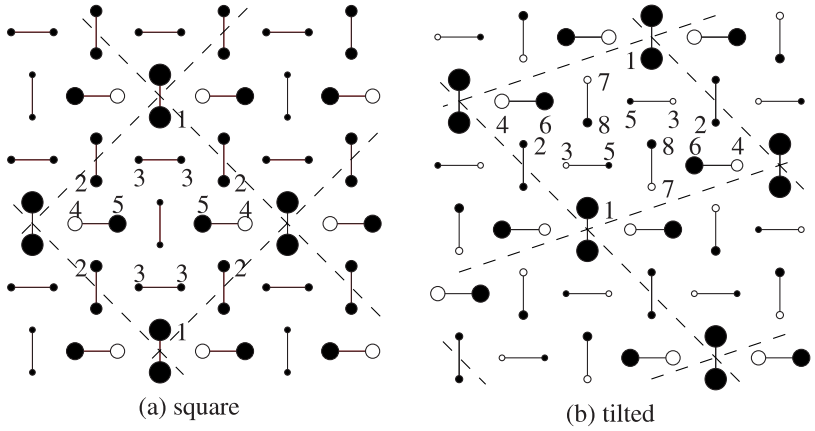

Figure 30. (a) Schematic distribution of magnetic moments at the 1/8 plateau for a square unit cell and (b) for a rhomboid unit cell. Full circles reveal the positive $\langle S^z \rangle$ sites and open circles the negative. Radii represent the magnitude of $\langle S^z \rangle$.

7. Conclusions

Low-dimensional spin systems have been studied intensively for a long time and many theoretical models, for example chain, zig-zag chain, ladder and others, have been considered. In the early stage of the investigations actual realizations for such models were very limited. However, thanks to the recent endeavours of chemists and experimentalists, many real materials whose behaviours are well explained by these simple models have been synthesized and have provided several interesting experimental results, which have in turn stimulated further theoretical development. $SrCu_2(BO_3)_2$ is one of the most fascinating examples. Over 20 years ago, Shastry and Sutherland found a two-dimensional model which has an exact ground state. But further theoretical developments of the model were not achieved for a long time. However, since the work of Kageyama *et al* on $SrCu_2(BO_3)_2$, many experimental and theoretical works have been developed as summarized in table 4. Through such works, many interesting phenomena, for example magnetization plateaux, have been found and convincing explanations given. In this way theories for this system have been developed by stimulations from the experiments and vice versa.

In this review, we have attempted to give an overview of the recent developments concerning the two-dimensional orthogonal dimer model of $SrCu_2(BO_3)_2$. The main conclusions are the following:

(i) In the two-dimensional orthogonal dimer model, the orthogonality of the dimer bonds plays an essential role. The exact dimer singlet ground state found by Shastry and Sutherland originates from this orthogonality. Such a point of view makes it easy to extend the dimer singlet ground state to other dimensions. The most remarkable fact is that the realistic three-dimensional model which corresponds to $SrCu_2(BO_3)_2$ has a dimer singlet ground state. Also the orthogonality is the origin of the almost localized nature of the triplet excitations. This property leads to the crystallization of triplet excitations at certain densities of the triplet excitations, which explains the magnetization plateaux at the corresponding magnetizations.

(ii) In the two-dimensional orthogonal dimer model, there is a quantum phase transition from the dimer singlet state to the antiferromagnetically ordered state. The plaquette singlet

Table 4. Theories on two-dimensional orthogonal dimer models and main phenomena discussed by them. Also the related section is indicated.

Method	Phenomenon	Section
Exact solution [36, 37]	Dimer singlet ground state	3.1
Schwinger boson mean field theory [49]	Quantum phase transitions	3.2.1
Exact diagonalization [35]	Quantum phase transitions	3.2.1
Series expansions [39, 46, 51, 54, 59]	Quantum phase transitions	3.2
Large-N limit with Sp($2N$) symmetry [50]	Quantum phase transitions	3.2.1
Field theory [53]	Quantum phase transitions	3.2.1
Dimer and quadrumer boson [52]	Quantum phase transitions	3.2.1
Perturbation calculation ($J'/J \ll 1$) [35]	Almost localized triplet	4.1
Exact diagonalization [35]	Almost localized triplet	4.1
Series expansion [46]	Almost localized triplet	4.1
Perturbative unitary transformation [58]	Almost localized triplet	4.1
Perturbation calculation ($D/J \ll 1$) [65]	Effect of DM interaction	4.1
Effective bosonic model [32]	Bound state of two triplets	4.2
Perturbation calculation ($J'/J \ll 1$) [63, 69]	Bound state of two triplets	4.2
Perturbative unitary transformation [58]	Bound state of two triplets	4.2
Exact diagonalization [63, 73]	Bound state of two triplets	4.2
Transfer matrix method [60]	Thermodynamic properties	5
Hard-core boson method [71, 72, 84, 86, 87]	Magnetization plateaux	6.1
Exact diagonalization [35]	Magnetization plateaux	6.1
Chern–Simons theory [88, 89]	Magnetization plateaux	6.2
Exact diagonalization [28, 95]	Effect of spin–phonon coupling	6.3

state probably exists between the two phases. A definitive conclusion about the third phase is still awaited.

(iii) The lowest branch of the triplet excitations is almost localized. Notice that the spin gap is not affected by the interlayer coupling J'' and the triplet excitations are localized along the c-axis direction. Therefore the low-temperature thermodynamic properties of $SrCu_2(BO_3)_2$ are well described by using the two-dimensional model as the first approximation, not because of the weakness of the interlayer coupling J'' but for geometrical reasons. Concerning the coupling constants J, J', and J'', the best fit for thermodynamic properties is obtained by $J = 85$ K, $J' = 54$ K and $J'' = 8$ K. These parameters show that $SrCu_2(BO_3)_2$ is located near the quantum phase transition point. The unusual temperature dependence of the susceptibility is a consequence of the closeness to the transition point.

(iv) There is a tendency for two-triplet excitations to make a bound state. Such a bound state hops more easily than the single-triplet excitations. The bound states are observed in many experiments and they are explained well by the theory, especially the results of the inelastic neutron scattering experiments. On the other hand, the selection rules for Raman and ESR experiments require further investigation.

(v) The almost localized triplet excitations can easily form regular lattices under certain magnetic fields. The commensurability energy associated with the superstructures leads to plateaux in the magnetization curve at 1/2, 1/3, 1/4 and 1/8 of the full moment. We would like to point out that $SrCu_2(BO_3)_2$ is the first example where magnetization plateaux accompanied by a lowering of the translational symmetry are observed.

(vi) We mention the importance of the coupling between spins and phonons. The spin–phonon interaction may be one of the interesting phenomena for $SrCu_2(BO_3)_2$. In the orthogonal dimer model, a finite matrix element for the hopping of a triplet arises when

the orthogonality is broken by some distortion of dimer bonds. This suggests that a triplet excitation has a strong coupling with phonons. In fact, the spin–phonon coupling is useful to lift up the degeneracy at magnetization plateaux.

Finally we point out the open issues related to $SrCu_2(BO_3)_2$:

(i) As mentioned in summary (ii) above, the properties of the intermediate phase of the orthogonal dimer model are not yet clear. Further investigation is required.
(ii) In this system, selection rules for Raman and ESR experiments are not yet clear. For ESR in particular the general theory in quantum spin systems is very limited. Since it is possible to measure an ESR signal in a high magnetic field with high accuracy, theoretical developments are necessary not only in this system but also in general quantum spin systems.
(iii) As proposed in [72], the nonplateau state at low magnetization might be a superfluid of bound states of two-triplet excitations. However, the features of the state at the nonplateau phase are not yet clear and further analysis of this state is required.
(iv) So far the $1/8$ plateau has been found only by phenomenological treatment. In that sense, the mechanism of stabilizing this plateau is not yet clear, although it is likely that this plateau stabilizes because of the long-range interactions.
(v) In the magnetization curve there are transitions from a plateau phase to a nonplateau phase. However, the order of the transition, first or second, is not clear. Also finite-temperature phase transitions in the plateau phases are expected and the order of such a phase transition is not yet known.
(vi) There is a possibility that spin–phonon coupling may play an important role in helping us understand various properties of this system. For example, the finite magnetization below the critical field (figure 3) and the discrepancy between the theory and the experiments for specific heat at $T \geqslant 15$ K may be understood using spin–phonon coupling.

Acknowledgments

The authors have benefited from long-term collaborations, discussions and exchange of ideas and results with a large number of people. We would especially like to express out sincere thanks to Hiroshi Kageyama for continuous discussions on experimental results. We thank Frederic Mila for many suggestions and comments for this article. We also thank Keisuke Totsuka and Federico Becca for many helpful discussions. We are also grateful to N Aso, C Berthier, Y Fukumoto, M Horvatić, K Kakurai, N Kawakami, K Kodama, A Koga, P Lemmens, B Lüthi, G Misguich, T Momoi, M Nishi, H Nojiri, K Onizuka, D Poilblanc, M Takigawa, Y Yamashita, and T Ziman for useful comments. SM was financially supported by the JSPS Research Fellowships for Young Scientists and by the Swiss National Fund. KU has been supported by Grant-in-Aid for Scientific Research on Priority Areas (B) from the Ministry of Education, Culture, Sports, Science and Technology.

References

[1] Haldane F D M 1983 *Phys. Lett.* A **93** 464
[2] Dagotto E and Rice T M 1996 *Science* **271** 618
[3] Lhuillier C and Misguich G 2001 Frustrated quantum magnets *Preprint* cond-mat/0109146
[4] Majumdar C and Ghosh D 1969 *J. Math. Phys.* **10** 1388
[5] Okamoto K and Nomura K 1992 *Phys. Lett.* A **169** 433
[6] Azuma M, Hiroi Z, Takano M, Ishida K and Kitaoka Y 1994 *Phys. Rev. Lett.* **73** 3463
[7] Iwase H, Isobe M, Ueda Y and Yasuoka H 1996 *J. Phys. Soc. Japan* **65** 2397

[8] Taniguchi S, Nishikawa T, Yasui Y, Kobayashi Y, Sato M, Nishioka T, Kontani M and Sano K 1995 *J. Phys. Soc. Japan* **64** 2758
[9] Hida K 1994 *J. Phys. Soc. Japan* **63** 2359
[10] Okamoto K 1995 *Solid State Commun.* **98** 245
[11] Tonegawa T, Nakao T and Kaburagi M 1996 *J. Phys. Soc. Japan* **65** 3317
[12] Totsuka K 1997 *Phys. Lett.* A **228** 103
[13] Oshikawa M, Yamanaka M and Affleck I 1997 *Phys. Rev. Lett.* **78** 1984
[14] Tonegawa T, Nishida T and Kaburagi M 1998 *Physica* B **246/247** 368
[15] Totsuka K 1998 *Phys. Rev.* B **57** 3454
[16] Darriet J and Regnault L P 1993 *Solid State Commun.* **86** 409
[17] Boucher J and Regnault L 1996 *J. Physique* I **6** 1939
[18] Isobe M and Ueda Y 1996 *J. Phys. Soc. Japan* **65** 3142
[19] Fujiwara N, Yasuoka H, Isobe M, Ueda Y and Maegawa S 1997 *Phys. Rev.* B **55** 11945
[20] Narumi Y, Hagiwara M, Sato R, Kindo K, Nakano H and Takahashi M 1998 *Physica* B **246/247** 509
[21] Smith R W and Keszler D A 1991 *J. Solid State Chem.* **93** 430
[22] Kageyama H, Yoshimura K, Stern R, Mushnikov N, Onizuka K, Kato M, Kosuge K, Slichter C, Goto T and Ueda Y 1999 *Phys. Rev. Lett.* **82** 3168
[23] Kageyama H, Onizuka K, Yamauchi T, Ueda Y, Hane S, Mitamura H, Goto T, Yoshimura K and Kosuge K 1999 *J. Phys. Soc. Japan* **68** 1821
[24] Kageyama H, Nishi M, Aso N, Onizuka K, Yosihama T, Nukui K, Kodama K, Kakurai K and Ueda Y 2000 *Phys. Rev. Lett.* **84** 5876
[25] Onizuka K, Kageyama H, Narumi Y, Kindo K, Ueda Y and Goto T 2000 *J. Phys. Soc. Japan* **69** 1016
[26] Kageyama H, Ueda Y, Narumi Y, Kindo K, Kosaka M and Uwatoko Y 2002 *Prog. Theor. Phys. Suppl.* **145**
[27] Oshikawa M 2000 *Phys. Rev. Lett.* **84** 1535
[28] Kodama K, Takigawa M, Horvatić M, Berthier C, Kageyama H, Ueda Y, Miyahara S, Becca F and Mila F 2002 *Science* **298** 395
[29] Kodama K, Yamazaki J, Takigawa M, Kageyama H, Onizuka K and Ueda Y 2002 *J. Phys.: Condens. Matter* **14** L319
[30] Kageyama H, Onizuka K, Ueda Y, Nohara M, Suzuki H and Takagi N 2000 *J. Exp. Theor. Phys.* **90** 129
[31] Nojiri H, Kageyama H, Onizuka K, Ueda Y and Motokawa M 1999 *J. Phys. Soc. Japan* **68** 2906
[32] Lemmens P, Grove M, Fischer M, Guntherodt G, Kotov V N, Kageyama H, Onizuka K and Ueda Y 2000 *Phys. Rev. Lett.* **85** 2605
[33] Rõõm T, Nagel U, Lippmaa E, Kageyama H, Onizuka K and Ueda Y 2000 *Phys. Rev.* B **61** 14342
[34] Sparta K *et al* 2001 *Eur. Phys. J.* **19** 507
[35] Miyahara S and Ueda K 1999 *Phys. Rev. Lett.* **82** 3701
[36] Shastry B S and Sutherland B 1981 *Physica* B **108** 1069
[37] Ueda K and Miyahara S 1999 *J. Phys.: Condens. Matter* **11** L175
[38] Sutherland B and Shastry B S 1983 *J. Stat. Phys.* **33** 477
[39] Koga A and Kawakami N 2000 *Phys. Rev. Lett.* **84** 4461
[40] Ivanov N and Richter J 1997 *Phys. Lett.* A **232** 308
[41] Richter J, Ivanov N and Schulenburg J 1998 *J. Phys.: Condens. Matter* **10** 3635
[42] Koga A and Kawakami N 2002 *Phys. Rev.* B **65** 214415
[43] Gelfand M 1991 *Phys. Rev.* B **43** 8644
[44] Surendran N and Shankar R 2002 *Phys. Rev.* B **66** 024415
[45] Chen S and Büttner H 2002 Exact ground state of the generalized three-dimensional Shastry—Sutherland model *Preprint* cond-mat/0201003
[46] Weihong Z, Oitmaa J and Hamer C J 1999 *Phys. Rev.* B **60** 6608
[47] Müller-Hartmann E, Singh R R P, Knetter C and Uhrig G S 2000 *Phys. Rev. Lett.* **84** 1808
[48] Manousakis E 1991 *Rev. Mod. Phys.* **63** 1
[49] Albrecht M and Mila F 1996 *Europhys. Lett.* **34** 145
[50] Chung C H, Marston J B and Sachdev S 2001 *Phys. Rev.* B **64** 134407
[51] Takushima Y, Koga A and Kawakami N 2001 *J. Phys. Soc. Japan* **70** 1369
[52] Läuchli A, Wessel S and Sigrist M 2002 *Phys. Rev.* B **66** 014401
[53] Carpentier D and Balents L 2002 *Phys. Rev.* B **65** 024427
[54] Weihong Z, Oitmaa J and Hamer C J 2002 *Phys. Rev.* B **65** 014408
[55] Ueda K, Kontani H, Sigrist M and Lee P A 1996 *Phys. Rev. Lett.* **76** 1932
[56] Troyer M, Kontani H and Ueda K 1996 *Phys. Rev. Lett.* **76** 3822
[57] Ferer M and Hmaid-Aidnejad A 1986 *Phys. Rev.* B **34** 6481

[58] Knetter C, Bühler A, Müller-Hartmann E and Uhrig G S 2000 *Phys. Rev. Lett.* **85** 3958
[59] Koga A 2000 *J. Phys. Soc. Japan* **69** 3509
[60] Miyahara S and Ueda K 2000 *J. Phys. Soc. Japan (Suppl.)* B **69** 72
[61] Kageyama H, Onizuka K, Ueda Y, Hane S, Mitamura H, Goto T, Yoshimura K and Kosuge K 1999 *Proc. 4th Int. Symp. on Advanced Physical Fields* pp 235–7
[62] Knetter C, Müller-Hartmann E and Uhrig G S 2000 *J. Phys.: Condens. Matter* **12** 9069
[63] Totsuka K, Miyahara S and Ueda K 2001 *Phys. Rev. Lett.* **86** 520
[64] Weihong Z, Oitmaa J and Hamer C J 1998 Series expansions for a Heisenberg antiferromagnetic model for $SrCu_2(BO_3)_2$ *Preprint* cond-mat/9811030
We use the results in table 1, which was omitted from their paper [46]
[65] Cépas O, Kakurai K, Regnault L P, Ziman J P B T, Aso N, Nishi M, Kageyama H and Ueda Y 2001 *Phys. Rev. Lett.* **87** 167205
[66] Miyahara S and Ueda K 2001 *J. Phys. Soc. Japan (Suppl.)* B **70** 180
[67] Els G, van Loosdrecht P H M, Lemmens P, Vonberg H, Güntherodt, Uhrig G S, Fujita O, Akimitsu J, Dhalenne G and Revcolevschi A 1997 *Phys. Rev. Lett.* **79** 5138
[68] Lemmens P, Fischer M, Els G, Güntherodt G, Mishchenko A S, Weiden M, Hauptmann R, Geibel C and Steglich F 1998 *Phys. Rev.* B **58** 14159
[69] Fukumoto Y 2000 *J. Phys. Soc. Japan* **69** 2755
[70] Nojiri H, Asano T, Ajiro Y, Kageyama H, Ueda Y and Motokawa M 2001 *Physica* B **294/295** 14
[71] Momoi T and Totsuka K 2000 *Phys. Rev.* B **61** 3231
[72] Momoi T and Totsuka K 2000 *Phys. Rev.* B **62** 15067
[73] Miyahara S, Totsuka K and Ueda K 2001 Magnetic excitation of orthogonal dimer Heisenberg spin system for $SrCu_2(Bo_3)_2$ *Proc. 11th Int. Conf. on Recent Progress in Many-Body Theories*
[74] Moriya T 1967 *J. Phys. Soc. Japan* **23** 490
[75] Fleury P A and Loudon R 1968 *Phys. Rev.* **166** 514
[76] Aso N, Kageyama H, Nishi M and Kakurai K 2003 unpublished
[77] Nojiri H, Kageyama H, Onizuka K, Ueda Y, Asano T, Ajiro Y and Motokawa M 2000 *J. Phys. Soc. Japan (Suppl.)* B **69** 83
[78] Kimura S, Hirai S, Narumi Y, Kindo K, Nojiri H, Kageyama H, Onizuka K and Ueda Y 2001 *Physica* B **294/295** 68
[79] Oshikawa M and Affleck I 2002 *Phys. Rev.* B **65** 134410
[80] Johnston D C 1996 *Phys. Rev.* B **54** 13009
[81] Kageyama H, Suzuki H, Nohara M, Onizuka K, Takagi H and Ueda Y 2000 *Physica* B **281/282** 667
[82] Kolezhuk A K 1999 *Phys. Rev.* B **59** 4181
[83] Momoi T, Sakamoto H and Kubo K 1999 *Phys. Rev.* B **59** 9491
[84] Miyahara S and Ueda K 2000 *Phys. Rev.* B **61** 3417
[85] Miyahara S and Ueda K 2000 *Physica* B **281/282** 661
[86] Fukumoto Y and Oguchi A 2000 *J. Phys. Soc. Japan* **69** 1286
[87] Fukumoto Y 2001 *J. Phys. Soc. Japan* **70** 1397
[88] Misguich G, Jolicoeur T and Girvin S M 2001 *Phys. Rev. Lett.* **87** 097203
[89] Jolicœur T, Misguich G and Girvin S M 2002 *Prog. Theor. Phys. Suppl.* **145**
[90] Lopez A, Rojo A G and Fradkin E 1994 *Phys. Rev.* B **49** 15139
[91] Kugel K I and Khomskii D I 1982 *Sov. Phys.–Usp.* **25** 231
[92] Zherlitsyn S, Schmidt S, Wolf B, Schwenk H, Lüthi B, Kageyama H, Onizuka K, Ueda Y and Ueda K 2000 *Phys. Rev.* B **62** 6097
[93] Wolf B, Zherlitsyn S, Schmidt S, Lüthi B, Kageyama H and Ueda Y 2001 *Phys. Rev. Lett.* **86** 4847
[94] Lüthi B, Wolf B, Zherlitsyn S, Schmidt S, Schwenk H and Sieling M 2001 *Physica* B **294/295** 20
[95] Miyahara S, Becca F and Mila F 2003 Theory of spin density profile in the magnetization plateaus of $SrCu_2(BO_3)_2$ *Preprint* cond-mat/0302332